HHS Public Access

Author manuscript

*J Pharm Sci*. Author manuscript; available in PMC 2020 October 01.

Published in final edited form as:

*J Pharm Sci*. 2019 October ; 108(10): 3443–3456. doi:10.1016/j.xphs.2019.04.019.

# Pre-incubation with everolimus and sirolimus reduces organic anion transporting polypeptide (OATP)1B1- and 1B3-mediated transport independently of mTOR kinase inhibition: implication in assessing OATP1B1- and OATP1B3-mediated drug-drug interactions

**Taleah Farasyn**,

Department of Pharmaceutical Sciences, University of Oklahoma Health Sciences Center, Oklahoma City, OK US

**Alexandra Crowe**,

Department of Pharmaceutical Sciences, University of Oklahoma Health Sciences Center, Oklahoma City, OK US

**Oliver Hatley**,

Certara UK Ltd, Simcyp Division, Level 2-Acero, 1 Concourse Way, Sheffield, S1 2BJ, United Kingdom

**Sibylle Neuhoff**,

Certara UK Ltd, Simcyp Division, Level 2-Acero, 1 Concourse Way, Sheffield, S1 2BJ, United Kingdom

**Khondoker Alam**,

[*]**Corresponding author**: Wei Yue, Reprint requests should be addressed to Wei Yue, 1110 N. Stonewall Avenue, Oklahoma City, OK 73117. wei-yue@ouhsc.edu. Phone: (405) 271-6593 Ext. 47828, Fax: (405) 271-7505.

Current address: Department of Pharmaceutical Sciences, University of Oklahoma Health Sciences Center College of Pharmacy, 1110 N. Stonewall Avenue, Oklahoma City, OK 73117.

Authorship Contributions

Participated in research design: TF, AC, WY

Conducted experiments: TF, AC, KA, JK

Contributed new reagents or analytic tools:

Performed data analysis: TF, AC, KD, SN, OH, JK, TL, WY

Wrote or contributed to writing the manuscript: TF, AC, SN, OH, TL, WY



This article contains supplementary material available via the internet at http://wileylibrary.com.

[1]·The American Association of Pharmaceutical Scientists (AAPS)/International Transport Consortium (ITC) Joint Workshop on Drug Transporters, Baltimore, MD, April 20–22, 2015, Farasyn, T., Pahwa, S., Ding, K., Alam, K., and Yue, W., Rapid Down-Regulation of Organic Anion Transporting Polypeptide (OATP) 1B1 and 1B3 Transport Function by Mammalian Target of Rapamycin (mTOR) Inhibitors.

[2]·Farasyn, T., Alam, K., Crowe, A., Neuhoff, S., Hatley, O., Wang, X., Zhang, P., Ding, K., Li, L. and Yue, W., Down-Regulation of OATP1B1-Mediated Transport by Mammalian Target of Rapamycin (mTOR) Inhibitors Everolimus and Sirolimus: Potential Mechanism and Implication in OATP-Mediated Drug-Drug Interactions, Experimental Biology Meeting, Chicago, IL, April, 2017

[3]·Farasyn, T., Alam, K., Crowe, A., Neuhoff, S., Hatley, O., Wang, X., Zhang, P., Ding, K., Li, L. and Yue, W., Assessing the OATP1B1- and OATP1B3-mediated drug-drug interaction potential of mammalian target of rapamycin (mTOR) inhibitor everolimus, 21st North American International Society for the Study of Xenobiotics (ISSX), Providence, RI, Sept., 2017

Department of Pharmaceutical Sciences, University of Oklahoma Health Sciences Center, Oklahoma City, OK US

**Jean Kanyo**,
Yale MS & Proteomics Resource, Yale University, New Haven, CT, US

**TuKiet Lam**,
Department of Molecular Biophysics and Biochemistry, Yale MS & Proteomics Resource, Yale University, New Haven, CT, US

**Kai Ding**,
Department of Biostatistics and Epidemiology, University of Oklahoma Health Sciences Center, Oklahoma City, OK US

**Wei Yue**
Department of Pharmaceutical Sciences, University of Oklahoma Health Sciences Center, Oklahoma City, OK US

## Abstract

Organic anion transporting polypeptides (OATP)1B1 and OATP1B3 mediate hepatic uptake of many drugs including lipid-lowering statins. Current studies determined the OATP1B1/1B3-mediated drug-drug interaction (DDI) potential of mammalian target of rapamycin (mTOR) inhibitors, everolimus and sirolimus, using R-value and physiologically based pharmacokinetic (PBPK) models. Pre-incubation with everolimus and sirolimus significantly decreased OATP1B1/1B3-mediated transport even after washing, and decreased inhibition constant values up to 8.3- and 2.9-fold for OATP1B1 and both 2.7-fold for OATP1B3, respectively. R-values of everolimus, but not sirolimus, were greater than the FDA recommended cut-off value of 1.1. PBPK models predict that everolimus and sirolimus have low OATP1B1/1B3-mediated DDI potential against pravastatin. OATP1B1/1B3-mediated transport was not affected by pre-incubation with INK-128 (10 μM, 1 h), which does however abolish mTOR kinase activity. The pre-incubation effects of everolimus and sirolimus on OATP1B1/1B3-mediated transport were similar in cells prior pre-incubated with vehicle control or INK-128, suggesting that inhibition of mTOR activity is not a prerequisite for the pre-incubation effects observed for everolimus and sirolimus. Nine potential phosphorylation sites of OATP1B1 were identified by phosphoproteomics; none of these are the predicted mTOR phosphorylation sites. We report the everolimus/sirolimus-pre-incubation-induced inhibitory effects on OATP1B1/1B3 and relatively low OATP1B1/1B3-mediated DDI potential of everolimus and sirolimus.

### Keywords

drug transport; drug interactions; organic anion-transporting polypeptide; transporters; hepatocytes; hepatic transport; pharmacokinetics; physiologically based pharmacokinetic modeling

## INTRODUCTION

Hepatic OATP1B1 and OATP1B3 are localized to the sinusoidal membrane of human hepatocytes and mediate the uptake of many clinically important drugs (e.g., lipid-lowering statins and anti-cancer agents)[1]. Decreased transport activity of OATP1B1 and OATP1B3 due to co-administered OATP inhibitors (e.g., cyclosporine [Cs] A) or genetic variation has been associated with increased systemic exposure of statins, statin-related myopathy, and even rhabdomyolysis[2,3]. The OATP1B1 c.521 T>C single nucleotide polymorphism has reduced transport function, and is the most robust and important predictor of statin-induced myopathy[3]. A static model using the R-value, which represents the predicted fold change in exposure of victim drug in the presence of a perpetrator drug, has been recommended by regulatory agencies to assess the OATP1B1- and OATP1B3-mediated DDI potential of inhibitors[4–6]. Assessing the *in vitro* inhibition constant ($K_i$) values against OATP1B1 and OATP1B3 is a critical step in model-based prediction of the DDI potential of perpetrator drugs/compounds. Several reports indicated that pre-incubation with some OATP inhibitors, including cyclosporine A, rifampicin, and dasatinib, decreases OATP1B1- and OATP1B3-mediated transport, resulting in reduced $K_i$ values[7–9]. Currently, the mechanism underlying the pre-incubation-induced reduction in OATP1B1 and OATP1B3 transport activity remains unknown. For CsA and rifampicin, the decreased $K_i$ values against OATP1B1 and OATP1B3 determined after inhibitor pre-incubation are close to the estimated *in vivo* $K_i$ values[8–10]. In the recently published US FDA draft guidance for OATP1B1- and OATP1B3-mediated DDI studies, a pre-incubation with the investigational compound was recommended when assessing the $K_i$ values *in vitro*[5].

Mammalian Target of Rapamycin (mTOR) inhibitors everolimus (EVR) and sirolimus (SIR) are immunosuppressant drugs that are frequently used in transplant patients[11,12]. In addition, EVR and SIR have anticancer effects[13–15]. EVR has been approved for the treatment of certain cancers[16], and SIR has been administered to transplant patients with cancers to achieve simultaneous immunosuppressant and anti-cancer effects[13–15]. Cardiovascular disease resulting from dyslipidemia is a common cause of illness and death in organ transplant recipients treated long-term with immunosuppressants[17]; therefore, immunosuppressant drugs, including EVR and SIR, are often co-administered with lipid-lowering statins in order to reduce the risk for cardiovascular disease in transplant patients[18]. Severe statin-related DDI cases were reported in transplant recipients and cancer patients concurrently using EVR or SIR with atorvastatin or simvastatin[19–22]. Because hepatic uptake processes have been reported as the rate-determining step of atorvastatin clearance, and systemic exposure of both atorvastatin and simvastatin acid has been reported in subjects with the c.521T>C polymorphism of OATP1B1[3,23], OATP inhibition can be expected to play a role in the reported DDIs. The previously reported $IC_{50}$ values for EVR and SIR against OATP1B1 and OATP1B3 transport function were determined without EVR or SIR pre-incubation in transporter-overexpressing stable cell lines[24]. Considering the recent recommendation from the US FDA draft guidance to include a pre-incubation step when determining the $K_i$ values *in vitro*, a re-evaluation of the OATP-mediated DDI potential of EVR and SIR after pre-incubation is warranted.

The mTOR kinase serves as the catalytic subunit of two multi-protein complexes, mTOR complex 1 (mTOR C1) and mTOR C2, which phosphorylate distinct downstream proteins[25]. EVR and SIR selectively inhibit the mTOR kinase activity of mTOR C1, but not mTOR C2[25], while some mTOR inhibitors, such as OSI-027[26] and INK-128[27], inhibit both mTOR C1 and mTOR C2 activity. OATP1B1 and OATP1B3 have putative phosphorylation sites by the mTOR kinase as predicted by the prediction of PK-specific phosphorylation (PPSP) software[28]. Thus, it is reasonable to hypothesize that impaired mTOR C1 kinase activity after pre-incubation with EVR or SIR is involved in regulating OATP1B1- and OATP1B3-mediated transport, presumably by altering phosphorylation of the transporters. The current studies were designed to determine the OATP1B1- and OATP1B3-mediated DDI potential of EVR and SIR, following the US FDA draft guidance and using static R-value and PBPK models. The involvement of impaired mTOR C1 kinase activity in the modulation of OATP1B1- and OATP1B3-mediated transport after EVR and SIR pre-incubation was also assessed.

## MATERIALS AND METHODS

### Materials.

[$^3$H]-cholecystokinin 8 (CCK-8) (specific activity 88.0 Ci/mmol), [$^3$H]-estradiol 17 β-D-glucuronide ($E_2$17βG) (specific activity 41.4 Ci/mmol) and [$^3$H]-estrone-3-sulfate ($E_1$S) (specific activity 54.0 Ci/mmol) were purchased from Perkin Elmer Life Science (Waltham, MA). [$^3$H]-rosuvastatin was purchased from American Radiolabeled Chemicals (St. Louis, MO). The radiochemical purities determined by Perkin Elmer via high-performance liquid chromatography are greater than 90%, 97%, and 97% for [$^3$H]-CCK-8, [$^3$H]-$E_1$S, and [$^3$H]-$E_2$17βG, respectively, and 99% for [$^3$H]-rosuvastatin. Radiochemical purity was not determined in-house before use; however, the radiolabeled compounds were used within a few months of purchase, and substrate accumulation in our control cells was comparable to data published previously[8,29]. EVR and SIR were purchased from LC laboratories (Woburn, MA). Unlabeled rosuvastatin was purchased from Toronto Research Chemicals (North York, ON, Canada). Unlabeled CCK-8, $E_2$17βG, dimethyl sulfoxide (DMSO), Hanks' Balanced Salt Solution (HBSS), Dulbecco's Modified Eagle Medium (DMEM), antibiotic antimycotic solution, Triton X-100, and trypsin-EDTA solution were purchased from Sigma-Aldrich (St. Louis, MO). Poly-L-lysine was purchased from Trevigen, Inc. (Gaithersburg, MD). Fetal bovine serum (FBS) was purchased from Hyclone Laboratories (Logan, Utah). Geneticin and HEPES buffer were obtained from Gibco (Life Technologies, Grand Island, NY). Bio-Safe II liquid scintillation mixture was purchased from Research Products International (Mt. Prospect, IL). Complete™ protease inhibitor cocktail (Roche Diagnostics, Indianapolis, IN). All other materials were purchased from Thermo Fisher Scientific (Waltham, MA).

### Cell culture.

Human embryonic kidney (HEK) 293 stable cell lines over-expressing OATP1B1 (HEK293-OATP1B1), OATP1B3 (HEK293-OATP1B3), and the HEK293-mock cell line were kindly provided by Dr. Dietrich Keppler[30,31]. The HEK293 stable cell line expressing FLAG-tagged WT-OATP1B1 was published previously[32]. These stable cell lines were maintained in complete DMEM medium supplemented with 10% FBS (v/v), 1% antibiotic antimycotic

solution, and 600 μg/ml Geneticin in a humidified atmosphere (95% $O_2$, 5% $CO_2$) at 37°C. HEK293-OATP1B1, HEK293-OATP1B3, and HEK293–mock cells were seeded at a density of $1.5 \times 10^5$ cells per well of a 24-well plate coated with poly-L-lysine and were allowed to grow for 48 h to confluence before the uptake studies were performed similarly to those we published previously[33].

### Inhibition and Uptake Studies.

The transport and inhibition studies were conducted similar to those described previously[8,34]. Three scenarios, pre-incubation, co-incubation, and co-incubation after a one-hour pre-incubation step (pre+co-incubation), were used to determine the effects of mTOR inhibitors EVR and SIR on OATP1B1 and OATP1B3-mediated transport. In the co-incubation scenario, without any pre-incubation, the uptake assay was performed and substrate accumulation was determined in the presence of vehicle control or inhibitors at the concentrations indicated in the figure legends. In the pre-incubation scenario, the cells were pre-incubated in complete culture medium containing either vehicle control, SIR, or EVR for the designated treatment times and at the concentrations indicated in the figure legends. After washing three times with HBSS buffer containing 10 mM HEPES (pH 7.4), substrate accumulation was determined in the absence of inhibitor. In the pre+co-incubation scenario, cells were first pre-incubated for one hour with either inhibitor or the vehicle control before the uptake assay was performed. Substrate accumulation was determined in the presence of the inhibitor or control at the same concentrations as those used in the pre- and co-incubation steps. DMSO (≤ 0.1%, v/v) was used as the vehicle control in all scenarios. CsA served as the positive control for the pre-incubation effects. To determine the long-lasting inhibitory effects of EVR on OATP1B1- and OATP1B3-mediated transport after EVR pre-incubation, HEK293-OATP1B1 and –OATP1B3 cells were pre-incubated with culture medium containing EVR (0.2 μM) or vehicle CTL for 1 h. At the end of pre-incubation, after washing three times with HBSS buffer, cells were cultured in fresh culture medium for up to 24 h.

[$^3$H]-$E_2$17βG (1 μM, 2 min), [$^3$H]-$E_1$S (25 nM, 0.5 min), and [$^3$H]-rosuvastatin (20 nM, 0.5 min) were used as probe substrates for OATP1B1 and [$^3$H]-CCK-8 (1 μM, 3 min) was used as the probe substrate for OATP1B3 in HEK293 stable cell lines overexpressing the transporter of interest, similar to that published previously[8,32,34]. The probe substrate concentrations used were below the reported $K_m$ values for OATP1B1 in HEK293 cells ($E_2$17βG - 8.29 μM, $E_1$S - 0.46 μM, and rosuvastatin - 0.8 μM; OATP1B3 [CCK-8 – 3.8 μM])[35,36] to ensure that the determined $IC_{50}$ value is approximately the same as the $K_i$ value. Substrate incubation times all fell within the linear uptake ranges as published previously[8,34] or determined in current studies (Supplemental Fig. S1)

At the end of the incubation with probe substrates in HBSS-HEPES buffer (pH 7.4), the uptake assay was terminated by aspirating the incubation buffer and washing the cells three times with ice-cold HBSS-HEPES buffer. Cells were lysed in 200 μL phosphate buffered saline (PBS) buffer containing 0.5% Triton-X 100. Substrate accumulation was determined by scintillation counting (LS6500 scintillation counter, Beckman Coulter, Brea, CA) and normalized to the protein concentration (~0.5 mg/mL) determined via BCA assay (Pierce

Chemical, Rockford, IL). The same uptake experiment for all substrates was conducted on a blank plate without cells in order to correct the accumulation values for nonspecific binding to the assay plate. For the experiments conducted with the substrates [$^3$H]-$E_2$17βG and [$^3$H]-rosuvastatin, OATP1B1-mediated uptake was calculated by performing the same experiments in HEK293-Mock cells and subtracting the values from those obtained in HEK293-OATP1B1, respectively. For other substrates, pilot experiments determined negligible accumulation in the HEK293-Mock cells, and inhibition was conducted in the transporter-expressing cells.

### Prediction of OATP-mediated DDIs using the static R-value model.

To determine the $IC_{50}$ values, the substrate accumulation was converted to percentage of the vehicle control and plotted against the inhibitor concentrations. The $IC_{50}$ values were estimated by nonlinear regression using the three-parameter model with GraphPad Prism v. 7.0 (GraphPad Software, La Jolla, CA) and are summarized in Table 1. The following equation was fit to the inhibition fold change vs. CTL-concentration data:

$$E=Bottom+(Top-Bottom)/(1+(C/IC_{50})) \quad \text{Eq. 1}$$

Weighing was not conducted for experimental values when fitting equation 1 to the data, as the dependent variable is not wide enough, justifying not using weighing. We have tested and found that weighing does not improve the $IC_{50}$ curve fitting. Based on the FDA draft guidance for *in vitro* DDI studies[5], the R-values, which represent the predicted ratio of the victim drug AUC in the presence and absence of the investigational drug, were calculated based on Eq. 2.

$$R=1+(f_{u,p}\times I_{in,max}/IC_{50}) \quad \text{Eq. 2}$$

$f_{u,p}$ is the unbound fraction of the inhibitor in the plasma. $I_{in,max}$ is the estimated maximum plasma concentration of the inhibitor at the inlet to the liver. The $I_{in,max}$ is calculated as:

$$I_{in,max}=I_{max}+(f_aF_g\times k_a\times Dose)/Q_h/R_B \quad \text{Eq. 3}$$

Where $I_{max}$ is the maximum plasma concentration of the inhibitor in systemic circulation, $f_a$ is the fraction absorbed, $F_g$ is the fraction that escapes intestinal metabolism, $k_a$ is the absorption rate constant, and $Q_h$ is the hepatic blood flow rate (1500 ml/min)[37]. $R_B$ is the blood-to-plasma concentration ratio. $f_aF_g$ and $k_a$ are currently unknown values so values of 1 and 0.1/min were used as worst-case estimates, respectively, as recommended by the FDA draft guidance[5]. The remaining parameters were obtained from the literature and are summarized in Supplemental Table S1.

### Pharmacokinetic Modeling and Simulations.

To evaluate the OATP1B1- and OATP1B3-mediated DDI potential of EVR and SIR against the OATP-substrate pravastatin, a PBPK modeling approach was designed utilizing the population-based Simcyp Simulator (version 17, SimCYP Ltd, Sheffield, UK). Our purpose in developing the EVR model is to assess, at the highest approved dose of EVR (10 mg), the OATP1B1- and OATP1B3-mediated DDI potential; hence, we used a clinical data from the 10-mg dose to develop the EVR model [38] and used other does (≤10 mg dose) to verify the model (reference summarized in supplemental Table S2). A fit-for-purpose PBPK perpetrator file of EVR was developed based on the parameters in Table 2.

The default pravastatin (Sim-Pravastatin) and midazolam (MDZ) PBPK models within the Simcyp Simulator library were used without modification, as published previously[33]. Use of the pravastatin PBPK model to assess OATP1B1 and OATP1B3-mediated DDIs was validated using rifampicin as the OATP1B1 and OATP1B3 inhibitor in our previous publication[33]. A previously published SIR PBPK model was used in the current study without modification[39].

EVR parameters are listed in Table 3. EVR is a neutral compound with a calculated n-octanol:water partition coefficient (Log $P_{O:W}$) of 4.23 as estimated using Advanced Chemistry Development software (ACD/Labs, Toronto, On, Canada)[40]. As the experimental Log P value of EVR has not been reported, the Log P value of EVR calculated using ACD software was used in the current study, similarly to that used in a previous publication[41]. At the blood concentration range of 5–100 ng/ml, EVR is bound to human erythrocytes with an erythrocyte binding of approximately 85%, while at blood concentrations higher than 100 ng/ml, the blood cell uptake of EVR was concentration-dependent[38]. Based on data described in the EVR clinical pharmacology and biopharmaceutics review, assuming a hematocrit value of 0.45, the EVR blood-to-plasma concentration ratio ($C_b/C_p$) was calculated as 3.4, 4.55, 4.58, 1.9, 1.1, and 0.71 at blood concentrations of 0.005, 0.05, 0.1, 0.5, 1, and 5 mg/L. The built-in model for the concentration-dependent $C_b/C_p$ within the Simcyp Simulator was used in the current study, employing the interpolation method. The unbound fraction of EVR in human plasma was determined to be 0.26[42]. The Simcyp advanced dissolution, absorption, and metabolism (ADAM) model[43] was used to describe the absorption with human jejunum effective permeability ($P_{eff,man}$) predicted using the mechanistic permeability (Mech Peff) model[44]. A liver-plasma concentration ratio ($K_{p,liver}$) value of 1 is assumed as a conservative default value for EVR since there is no reported evidence of EVR hepatic uptake. Furthermore, as the systemic concentrations of EVR are the driving concetrations for interactions with hepatic uptake transporters OATP1B1 and OATP1B3, the emphasis for this fit-for-purpose minimal PBPK model of EVR is the systemic concentrations. Sensitivity analysis has shown that the systemic concentrations of EVR were insensitive to changes to $K_{p,liver}$ (Supplemental Fig. S2 A–D).

A minimal PBPK model with a single-adjusting peripheral compartment (SAC) was used to describe the distribution of EVR based upon the ability to consider the observed concentration dependency in the blood-to-plasma ratio (Table 2). Non-linearity observed in doses higher than 10 mg was not addressed. The elimination of EVR was described using an oral clearance value of 15.4 L/h (34.3% CV) after a dose of 10 mg once per day at steady

state[38]. Renal clearance of EVR was set to 0 based on the fact that, in humans, detection of the EVR parent drug in the urine was negligible[45]. It has been reported previously that transport of EVR in the basolateral-to-apical transport direction of Caco-2 monolayers was ~20 fold greater than in the apical-to-basolateral transport direction, and that the P-gp inhibitor verapamil completely inhibited the efflux of EVR [46], suggesting EVR is a substrate of P-gp. Thus, a P-gp-mediated intestinal efflux intrinsic clearance of 7 μl/min/cm$^2$ was incorporated into the current PBPK model as the best fit value describing the reported steady state $C_{max}$ (76.7 ng/mL) of EVR following once daily 10 mg doses[47] and the $C_{max}$ of EVR following weekly dose at 10 mg[38]. MDZ is a substrate of CYP3A[48], and EVR is a inhibitor of CYP3A[47]. The application of the EVR PBPK model to predict internal hepatic interactions was independently verified using a clinical DDI study wherein co-administration of 10 mg EVR at steady state with a single 4 mg dose of MDZ increased the observed AUC and $C_{max}$ ratios of midazolam by 1.30 and 1.25 fold, respectively[49]. No sensitivity of MDZ AUC and $C_{max}$ to $K_{p,liver}$ was observed over a 100 fold range; therefore, the default $K_{p,liver}$ of 1 was maintained (Supplemental Fig. S2 E and F).

Since pravastatin is minimally metabolized through CYP450 enzymes[50], the DDI simulation of EVR against pravastatin was performed on a fit-for-purpose basis assuming that EVR affects the disposition of pravastatin only through the inhibition of OATP1B1 and OATP1B3[5]. Although pravastatin is also a substrate of OATP2B1[51], OATP1A2[52], and MRP2[53–55], inhibition of EVR and SIR on OATP2B1 and MRP2 has not been reported. OATP1A2 mRNA is expressed at a low level[56] or could not be detected[5758] along the small intestine, and several laboratories were not able to determine OATP1A2 protein in intestinal samples[59–61]. In addition, scalable *in vitro* data for OATP1A2 kinetics for pravastatin are currently not available. Hence, the inhibition of OATP1A2 by EVR and SIR in the intestine is currently not specifically implemented in the pravastatin model. EVR and SIR have been reported to inhibit OATP1A2[24]. As OATP1A2 is not specifically considered in the Simcyp pravastatin default model due to the lack of abundance and scalable *in vitro* kinetics data, the effects of EVR and SIR on OATP1A2 were therefore not considered when assessing the DDIs against pravastatin. After multiple doses of EVR at the highest FDA-approved 10 mg daily dose, steady state was reached at around 7 days[38]. As the steady-state AUC of EVR is approximately 1.5 fold higher than that of the single dose AUC[38], the DDI simulation of EVR against pravastatin was performed in a 7-day trial in 100 virtual subjects (10 trials × 10 subjects) using the default Sim-Healthy volunteer data library. After multiple twice daily doses of 0.5 – 6.5 mg/m$^2$ SIR (equivalent to ~1 – 12.5 mg) in stable renal transplant patients, steady state was achieved at around day 5–7 at all doses[62]. The highest recommended dose for SIR in patients at high-immunologic risk is a loading dose of up to 15 mg on day one, followed by daily maintenance doses of 5 mg[11]. The DDI trial design, therefore, was comprised of the highest recommended dose of SIR (15 mg) co-administered daily with 40 mg pravastatin each day for 7 days to ensure that the inhibitor reaches steady state. The DDI simulation for SIR was also performed in 100 virtual subjects (10 trials x 10 subjects) using the default Sim-Healthy volunteer data library.

CsA is a potent OATP1B1 and OATP1B3 inhibitor and was used as calibrator compound to assess OATP-mediated DDIs in the current studies, as published previously[8]. A sensitivity analysis was conducted to assess the impact of the *in vitro* determined $K_i$ value of EVR and

SIR against OATP1B1 and OATP1B3 on the estimated AUC ratio (AUCR) of pravastatin. Four potential modeling scenarios were assessed: direct use of measured *in vitro* pre+co-$IC_{50}$ values (I); assuming saturated *in vitro* conditions $K_i$ values were half of the measured pre+co-$IC_{50}$ values (II) (although the experimental conditions used were already accounting for this, this was only included as it is often used as a 'worst case' scenario); CsA-calibrated pre+co-$IC_{50}$ (III) and half of the pre+co-$IC_{50}$ values (IV) according to equation 5.

$$\text{Calibrated } K_{i,OATP,EVR/SIR} = \textit{in vitro}\ K_{i,OATP,EVR/SIR} * (\textit{in vivo}\ K_{i,OATP,CsA})/(\textit{in vitro}\ K_{i,OATP,CsA}) \quad \text{Eq. 5}$$

Where *in vivo* $K_{i,OATP,CsA}$ values are the estimated *in vivo* $K_i$ values for CsA against OATP1B1 (0.019 μM) and OATP1B3 (0.032 μM)[63]. The *in vitro* $K_{i,OATP,\ EVR/SIR}$ were $IC_{50}$ values summarized in Table 1. For OATP1B1, where multiple probe substrates were used to determine the $IC_{50}$ values, the lowest $IC_{50}$ value was used for the simulation. The *in vitro* $K_{i,OATP,CsA}$ are the $IC_{50}$ values determined for CsA in the current studies (Supplemental Fig. S3).

## Transport kinetics.

The maximal transport velocity ($V_{max}$) and the affinity constant ($K_m$) of OATP1B1-mediated transport of $E_2$17βG (0.1–40 μM, 2 min) and OATP1B3-mediated transport of CCK-8 (0.01–40 μM, 3 min) were determined in HEK293–1B1 and HEK293–1B3 cells, respectively, similarly to that published previously[8,29]. $V_{max}$ and $K_m$ values were determined in cells pre-incubated with 1 μM EVR, SIR, or vehicle control (CTL) for 1 hour and washing, or cells without pre-incubation.

The $V_{max}$ and $K_m$ values of $E_2$17βG and CCK-8 transport were estimated by fitting the Michaelis–Menten equation below to the data using GraphPad Prism v.7.0 (GraphPad Software, La Jolla, CA, USA), where v is the transport velocity of substrates and S is the substrate concentration.

$$v=\frac{V_{max}*S}{K_m+S}$$

## Immunoprecipitation and immunoblotting

Immunoprecipitation of FLAG-OATP1B1 and immunoblotting was performed similarly to that published previously[29]. In brief, after immunoprecipitation with FLAG antibody (F1804, Sigma Aldrich, St. Louis, MO) and subsequent washing, denatured whole cell lysates (WCLs) (50 μg) or immunocomplex were resolved on a 10% SDS-PAGE gel (Bio-Rad, Hercules, CA). Immunoblots were probed with antibodies from Cell Signaling Technology (Danvers, MA): p70 S6 kinase (S6K) (49D7, 1:1000 dilution), phosphor-p70S6K (108D2, 1:1000), Phospho (p)-Akt (Ser473) (D9E) (1:2000 dilution), pan AKT (C67E7, 1:2000), and from Sigma-Aldrich, St. Louis, MO: β-actin (1:5000). After incubation with respective secondary antibody conjugated with horseradish peroxidase

(1:5000, Santa Cruz Biotechnology, Inc., Dallas, Texas), signal was detected using Supersignal West Duro (Pierce, Rockford, IL) on a Bio-Rad ChemiDoc XRS imaging system (Bio-Rad Laboratories, Hercules, CA). Image Lab Software (Bio-Rad Laboratories, Hercules, CA) was used for densitometry. The SDS-PAGE with immunoprecipitated FLAG-OATP1B1 was stained with Coomassie Blue for subsequent phosphoproteomics analysis.

### Phosphoproteomics by liquid chromatography tandem mass spectrometry (LC-MS/MS).

FLAG-OATP1B1 proteins were purified from 20 dishes (100 mm) of HEK293-FLAG1B1 cells by immunoprecipitation with FLAG antibody, as described above. Gel bands of FLAG-OATP1B1 from SDS-PAGE stained with Coomassie Blue were excised for subsequent phosphoproteomic analysis. In-gel trypsin digestion and subsequent phosphoproteomics studies by LC-MS/MS were conducted at the MS and Proteomics Resource of the WM Keck Foundation Biotechnology Resource Laboratory at Yale, USA (see Supplemental Experimental Procedures for details in MS analysis).

### Statistics.

As indicated in the relevant figure legends, fold changes and associated standard errors (SEs) of substrate accumulation in treatment group(s) vs. control were estimated using generalized linear mixed models with the log link function, a fixed group effect and a random effect, while adjusting for group-specific over-dispersion. In cases of multiple comparisons, p-values were adjusted based on the Bonferroni's method. A two-sided p-value of $\leq 0.05$ defines statistical significance. The SAS software (version 9.3, Cary, NC) was used for statistical analyses.

## RESULTS

### Effects of EVR- and SIR-pre-incubation on OATP1B1- and OATP1B3-mediated transport.

After pre-incubation with EVR, SIR, or vehicle control and subsequent washing, OATP1B1- and 1B3-mediated transport was determined in the absence of EVR and SIR in HEK293-OATP1B1 and -OATP1B3 stable cell lines, respectively. After pre-incubation with EVR or SIR (both 0.2–5 μM) for 10 min, 30 min, and 1 h, OATP1B1-mediated [$^3$H]-$E_2$17βG transport (1 μM, 2 min) was significantly decreased, ranging 0.72 ± 0.03 – 0.12 ± 0.02 and 0.91 ± 0.02 – 0.20 ± 0.02 fold of vehicle control ($p<0.001$) for EVR (Fig. 1 A) and SIR (Fig. 1 B), respectively. One hour of pre-incubation with EVR (0.1 or 0.2–10 μM) or SIR (0.1–5 μM) also significantly decreased OATP1B1-mediated transport of [$^3$H]-$E_1$S (25 nM, 0.5 min) (Fig. 1 C and D) and [$^3$H]-rosuvastatin (20 nM, 0.5 min) (Fig. 1 E and F) in a concentration-dependent manner ($p<0.001$). After pre-incubation with EVR or SIR (both 0.2–5 μM) for 10 min, 30 min, and 1 h, OATP1B3-mediated [$^3$H]-CCK-8 transport (1 μM, 3 min) was significantly decreased, ranging 0.81 ± 0.04 – 0.17 ± 0.03 and 0.86 ± 0.04 – 0.29 ± 0.04 fold of vehicle control ($p<0.001$) for EVR (Fig. 1 E) and SIR (Fig. 1 F), respectively.

As the concentration-dependent pre-incubation effects of EVR and SIR on OATP1B1- and OATP1B3-mediated transport of [$^3$H]-$E_2$17βG and [$^3$H]-CCK-8 appear to be the greatest at one hour, a 1-h pre-incubation time point was chosen in subsequent studies to determine the effects of EVR- and SIR-pre-incubation on $IC_{50}$ values of EVR and SIR against OATP1B1-

and OATP1B3-mediated transport. The LDH assay showed negligible toxicity in HEK293-OATP1B1 and HEK293-OATP1B3 cell lines following one hour pre-incubation with EVR (0.001–10 μM) or SIR (0.01 – 5 μM) (Supplemental Fig. S4).

### Effects of EVR- and SIR-pre-incubation on $IC_{50}$ values of EVR and SIR against OATP1B1- and OATP1B3-mediated transport.

$IC_{50}$ values of EVR and SIR against OATP1B1-mediated transport of [$^3$H]-$E_2$17βG, [$^3$H]-$E_1$S and [$^3$H]-rosuvastatin and OATP1B3-mediated transport of [$^3$H]-CCK-8 was determined under co-incubation with EVR or SIR with or without 1 h pre-incubation with EVR or SIR (Fig. 2 and Table 1).

Pre-incubation for one hour followed by co-incubation (pre+co-incubation) with EVR significantly decreased the $IC_{50}$ values of EVR against OATP1B1-mediated transport of [$^3$H]$E_2$17βG, [$^3$H]-$E_1$S and [$^3$H]-rosuvastatin by 2.1, 3.8, and 8.3 fold, respectively, and against OATP1B3-mediated transport of [$^3$H]-CCK-8 by 2.7 fold, compared with co-incubation with EVR only ($p<0.05$ by t-test, n=3 in triplicate, Fig. 2 A–D, and Table 1). SIR pre+co-incubation decreased the $IC_{50}$ values of SIR against OATP1B1-mediated transport of [$^3$H]-$E_2$17βG, [$^3$H]$E_1$S, and [$^3$H]-rosuvastatin by 2.9, 1.5, and 1.8 fold, respectively. However, the observed reduction in the SIR $IC_{50}$ values for OATP1B1 did not reach a statistically significant level. SIR pre+co-incubation significantly decreased the $IC_{50}$ of SIR against OATP1B3-mediated transport of [$^3$H]-CCK-8 by 2.9 fold compared with co-incubation with SIR ($p<0.05$ by t-test, n=3 in triplicate). Pre-incubation with the positive control CsA also reduced the $IC_{50}$ values against OATP1B1- and OATP1B3- mediated substrate transport (Supplemental Fig. S3 A and B).

### Prediction of OATP-mediated DDIs using static R-value and PBPK modeling.

EVR and SIR R-values determined against OATP1B1 and OATP1B3 are summarized in Table 1. For EVR, the R-values against OATP1B1 and OATP1B3 were 1.19 – 1.27 and 1.23, respectively, using the pre+co-incubation $IC_{50}$ values, and were 1.03 – 1.09 and 1.09, respectively, using the co-incubation $IC_{50}$ values. Using $IC_{50}$ values published previously without EVR pre-incubation [24], the R values were 1.01 for both OATP1B1 and OATP1B3. For SIR, using the lowest $IC_{50}$ values determined in current and previous studies [24], the R-values were all 1.

The EVR PBPK model well described the blood concentration profile of EVR administered to patients at weekly doses of 10 mg (Fig. 3 A), which is the clinical data used to develop the model [38]. This model also well described other clinical data at different doses (Fig. 3 B and Supplemental Table S2 and Figs S10–S16). The EVR model was then verified by an independent clinical DDI study of EVR against MDZ[49]. The MDZ PBPK model well described the plasma concentration-time profile of MDZ [49] (Supplemental Fig. S5). The simulated AUC and $C_{max}$ ratios of MDZ when co-administered with 10 mg EVR were 1.15 and 1.13, respectively (Supplemental Fig. S5), comparable to the clinical data of 1.30 and 1.25, respectively[49]. These data suggest that the predictive performance of the EVR model can be verified by an independent clinical study. Using the CsA-calibrated pre+co-incubation $IC_{50}$ values of OATP1B1 and OATP1B3, the AUC and $C_{max}$ ratios of pravastatin

predicted following the 7-day trial of 10 mg daily doses of EVR and a 40 mg daily dose of pravastatin were 1.04 and 1.06, respectively (Supplemental Table S3). Using half of the CsA-calibrated pre+co-$IC_{50}$ values of EVR against OATP1B1 and OATP1B3 as a worst-case scenario, the predicted pravastatin AUC and $C_{max}$ ratios were 1.10 and 1.18, respectively (Fig. 3 D and Supplemental Table S3).

The SIR PBPK model [64] well described the observed blood concentration profile of SIR after a 5 mg/$m^2$ single dose (Fig. 3 C). Under the worst-case scenario using half of the pre +co-$IC_{50}$ values calibrated by CsA, the predicted AUC and $C_{max}$ ratios of pravastatin (administered at 40 mg once per day) were both 1.0, when co-administered for 7 days with the highest US FDA-approved SIR dose of 15 mg (Fig. 3 D and Supplemental Table S3).

### Effects of EVR and SIR on transport kinetics of OATP1B1- and OATP1B3.

The effects of EVR and SIR pre-incubation (1 μM, 1 h) on the $V_{max}$ and $K_m$ values of OATP1B1- and OATP1B3-mediated transport were determined in HEK293–1B1 and HEK293–1B3 cells, respectively (Fig. 4 and Table 3). Pre-incubation with EVR or SIR (1 μM, 1 h) significantly increased the $K_m$ values for OATP1B1-mediated [$^3$H]$E_2$17βG transport (3.3 ± 1.3, 9.7 ± 1.8, and 9.2 ± 4.3 μM for CTL, EVR and SIR, respectively), and significantly decreased the $V_{max}$ values (46.9 ± 11.8, 32.3 ± 9.0, and 31.9 ± 5.1 pmol/mg protein/min for CTL, EVR, and SIR, respectively). The $K_m$ values for OATP1B3-mediated [$^3$H]CCK-8 transport were also significantly increased after pre-incubation with EVR or SIR (5.8 ± 2.1, 24.2 ± 8.7, and 22.9 ± 8.5 μM for CTL, EVR, and SIR, respectively). The $V_{max}$ values for OATP1B3 were not significantly affected by EVR or SIR pre-incubation (49.8 ± 16.6, 39.9 ± 3.8, and 50.5 ± 5.3 pmol/mg protein/min for CTL, EVR, and SIR). Without pre-incubation, co-incubation with EVR or SIR (both 5 μM) increased $K_m$ values of OATP1B1 by 6–10 fold, while it had minimal effect (1.2–1.7 fold vs. CTL) on $V_{max}$ (Supplemental Fig. S6).

### Long-lasting inhibitory effects of EVR on OATP1B1- and OATP1B3-mediated transport.

After 1 h pre-incubation with EVR (0.2 μM), OATP1B1-mediated transport of [$^3$H]rosuvastatin was significantly decreased to 0.54 ± 0.07 fold of control (Fig 5 A). OATP1B3-mediated transport of [$^3$H]CCK-8 was significantly decreased to 0.76 ± 0.05 fold of control (Fig 5 B). For OATP1B1-mediated transport, after washing off the EVR and culture in fresh medium, rosuvastatin accumulation was still significantly decreased even at 4 h (0.87 ± 0.03 fold of CTL, $p<0.05$). For OATP1B3-mediated transport, at 4, 6, and even 22 h after culturing cells in EVRfree medium after washing, [$^3$H]CCK-8 accumulation in EVR-pre-incubated cells remained significantly decreased when compared with the cells pre-incubated with vehicle control (0.76 ± 0.04, 0.73 ± 0.04 and 0.81 ± 0.06 fold of CTL, respectively, $p<0.05$ at each time point).

### Pre-incubation effects of EVR and SIR on OATP1B1- and OATP1B3-mediated transport in cells with and without mTOR kinase activity.

We next tested whether the pre-incubation-induced inhibitory effects of EVR and SIR on OATP1B1- and OATP1B3-mediated transport are related to their mTOR C1 kinase inhibition activity. The effects of EVR and SIR on OATP1B1 and OATP1B3-mediated

transport were compared in control cells with regular mTOR kinase activity and in cells in which mTOR C1 kinase activity was abolished by INK-128 prior to EVR and SIR pre-incubation. Phosphorylation of p70S6K at T389 and of AKT at S473 was used as a read out of mTOR C1 and C2 activity, respectively, similar to that published previously[65–67].

In HEK293-OATP1B1 cells, compared with vehicle control treatment, pre-incubation with EVR (0.2 μM, 1 h ) or SIR (0.5 μM, 1 h ) markedly reduced the amount of phosphorylated p70S6K at T389 [P-p70s6k (T389)] without affecting protein levels of total p70S6k, as determined by immunoblotting with an antibody specific for phosphorylated p70S6k at T389 and total p70S6k, respectively (Fig. 6 A). Pre-incubation with EVR (0.2 μM, 1 h ) or SIR (0.5 μM, 1 h ) did not inhibit either the amount of phosphorylation of AKT at S473 or total AKT protein levels (Fig. 6 A). Pre-incubation with mTOR C1 and C2 dual inhibitor INK-128 (10 μM, 1 h) alone or in combination with EVR (0.2 μM) or SIR (0.5 μM) markedly reduced both phosphor-AKT (S473) and phospho-p70S6K (T389), without affecting total protein levels of either protein (Fig. 6 B). Similar effects of EVR, SIR ,and INK-128 on phosphorylated and total p70s6k and AKT were observed in HEK293-OATP1B3 cells (Supplemental Fig. S7 and S8).

In HEK293-OATP1B1 and HEK293-OATP1B3 cells, incubation with INK-128 (10 μM, 1 h) did not significantly affect OATP1B1- (Fig. 7 A) or OATP1B3-mediated transport (Fig. 7 B), compared with vehicle control pre-incubation. Pre-incubation with EVR (0.2 μM, 1 h) or SIR (0.5 μM, 1 h) alone significantly decreased OATP1B1-mediated transport to 0.67 ± 0.02 or 0.60 ± 0.05 fold of control (Fig. 7 A) and OATP1B3-mediated transport to 0.60 ± 0.03 or 0.49 ± 0.03 fold of control (Fig. 7 B), respectively. Compared with pre-incubation with EVR (0.2 μM, 1 h) or SIR (0.5 μM, 1 h) alone, there was no significant difference in accumulation of [$^3$H]-$E_2$17βG (Fig. 7 A) or [$^3$H]-CCK-8 (Fig. 7 B) in cells pre-incubated with INK-128 (10 μM, 1 h) prior to EVR or SIR.

### Identification of phosphorylation sites in OATP1B1.

A total of 9 potential phosphorylation sites, S293, S295, T301, T439, T441, Y442, Y590, S659 and S663, were identified on OATP1B1 from our phosphoproteomics experiments (Table 4). The measured mass for all phosphopeptides included in Table 4 had absolute mass accuracy values of less than 4 ppm, indicating accurate peptide assignments. Six phosphorylation sites (S293, T439, T441, Y442, S659, S663) are associated with phosphopeptides with high Mascot Scores of above 67, indicating that the null hypothesis that the observed match is a random event had a probability of less than 5%[68]. Although S295, T301, and Y590 had Mascot Scores less than 67 (62.56, 29.22, and 35.59, respectively), their peptide fragmentation pattern and identity of the phosphopeptides were manually confirmed. Six sites (S293, S295, T301, Y590, S659, S663) had PhosphoRS probability[69] values near 100%, suggesting that these six sites were confidently identified as phosphorylation sites. Manual verification also confirmed that the above six sites are phosphorylation sites, as exemplified in Supplemental Fig. S9. However, localization of one phosphorylation site among the T439, T441, and Y442 residues on the same phosphopeptide cannot be verified, as these three sites exist on the same ion fragment with only one site being phosphorylated. The PhosphoRS probability value of ~33.33% for each of these three

sites suggests that there was equal probability for any one of these sites to be phosphorylated. In summary, six phosphorylation sites (S293, S295, T301, Y590, S659, S663) were identified on OATP1B1 with high confidence. Three potential phosphorylation sites, T439, T441, and Y442, need to be further characterized.

## DISCUSSION

The current study reports the rapid reduction of OATP1B1- and OATP1B3-mediated transport following pre-incubation with mTOR inhibitors EVR and SIR. The OATP-mediated DDI potential of EVR and SIR was then assessed using the static R-value model published in the US FDA draft guidance for *in vitro* OATP-mediated DDI studies in combination with PBPK modeling. The potential role of inhibition of mTOR C1 kinase in the pre-incubation effects was also evaluated.

Pre-incubation with 0.2–5 μM EVR rapidly and significantly decreased OATP1B1- and OATP1B3-mediated transport as early as ten minutes after beginning the incubation (Fig. 1). Pre-incubation with EVR for one hour significantly decreased the $IC_{50}$ values against OATP1B1 and OATP1B3 and led to increased R-values for OATP-mediated DDI prediction (Table 1). Coincubation of EVR with three OATP1B1 substrates ($E_2$17βG, $E_1$S, or rosuvastatin) or the specific OATP1B3 substrate CCK-8 yielded $IC_{50}$ values ranging from 0.48 ± 0.07 ($E_2$17βG) to 1.58 ± 0.92 (rosuvastatin) for OATP1B1 and 0.51 ± 0.08 μM for OATP1B3 (Table 1). Pre-incubation followed by co-incubation with EVR reduced the $IC_{50}$ values against OATP1B1 2.1, 3.8, and 8.3 fold for $E_2$17βG, $E_1$S, and rosuvastatin, respectively, and ~2.7 fold for OATP1B3 (Table 1). Using the pre+co-incubation $IC_{50}$ values recommended by the US FDA, R-values of EVR against OATP1B1 and OATP1B3 were all above the US FDA recommended cut-off value of 1.1, ranging from 1.19 ($E_2$17βG) −1.27 ($E_1$S). Hence, the static R-value model predicts that EVR has potential to cause OATP1B1- and OATP1B3-mediated DDIs. We further conducted PBPK modeling to assess the OATP1B1- and OATP1B3-mediated DDI potential of EVR. A previously reported single dose clinical DDI study indicated that co-administration of 2 mg EVR did not influence the pharmacokinetics of pravastatin to a clinically relevant extent in healthy volunteers (Zortress, 2010). Consistent with the findings of this clinical study, a DDI simulation of 2 mg EVR with single dose pravastatin (20 mg) yielded an AUC and $C_{max}$ ratio of 1.0 (data not shown). The highest approved dose of EVR is 10 mg in cancer patients; however, the effect of 10 mg EVR on the pharmacokinetics of OATP drug substrates (e.g., pravastatin) has not been reported in a clinical study. Our simulation results indicate that even using the lowest worst-case scenario $IC_{50}$ values, which are the half of the pre+co-incubation $IC_{50}$ values after calibration with CsA (scenario 4), the AUC and $C_{max}$ ratios of pravastatin when co-administered with EVR were 1.10 and 1.18, respectively (Fig. 3 D), suggesting that EVR has low potential to cause OATP-mediated DDIs. However, in transplant recipients who received EVR treatment (2.5 ± 1.0 mg per day) for at least three months prior to a one-month concomitant treatment with EVR and rosuvastatin, the rosuvastatin AUC and $C_{max}$ was ~2.8 and ~2.5 fold higher than the literature data in healthy volunteers [70,71]. Currently, the mechanism underlying the discrepancy between the predicted DDI potential in the current study and the observed clinical DDI of EVR against rosuvastatin[70] remains unknown. Here, we reported that after EVR pre-incubation and washing, the inhibitory

effects of EVR on OATP1B1 and OATP1B3 last up to 4 and 22 hs. Such longlasting inhibition characteristics of EVR may contribute to underestimated DDI prediction.

Pre-incubation with SIR also rapidly and significantly decreased OATP1B1- and OATP1B3-mediated transport (Fig. 1) and reduced the $IC_{50}$ against OATP1B1 ~2.9, 1.3, and 1.8 fold for $E_2$17βG, $E_1$S and rosuvastatin, respectively, and ~2.7 fold for OATP1B3 (Fig. 2 and Table 1). However, the static R-value and PBPK models both predict no change in the victim drug AUC, suggesting that the OATP1B1- and OATP1B3-mediated DDI potential for SIR is low. Cases of severe rhabdomyolysis, and even death, have been reported in solid-organ transplant patients concurrently administered SIR with simvastatin or fluvastatin [22,72,73]. Both simvastatin and fluvastatin are extensively metabolized by CYP3A[74,75], and SIR has been reported as a CYP3A inhibitor[76]. Though the OATP1B1 c. 521 T>C polymorphism is associated with increased systemic concentrations of simvastatin and simvastatin-induced toxicity, in the reported DDIs involving SIR and simvastatin, potential involvement of metabolic inhibition is also possible. To the best of our knowledge, neither adverse events nor clinical studies of SIR against metabolically stable statins have been reported to date. Alternatively, in the case report published by Hong et al., the transplant patient in question was initially treated with CsA as the main immunosuppressant and was switched due to the combined immunosuppressant and anticancer benefits of sirolimus therapy[22]. A few weeks after changing the immunosuppressive agent, the patient was admitted to the hospital with severe adverse effects, including rhabdomyolysis. Considering that CsA has been reported to inhibit OATP in a long-lasting manner even after removal of the drug[77], it can be assumed that CsA also plays a potential role in this DDI. Based on the DDI prediction from the current study, it is unlikely that SIR alone will cause OATP1B1- and OATP1B3-mediated DDIs when co-administered with metabolically stable statins.

In an effort to elucidate the potential mechanism underlying the pre-incubation-induced reduction of OATP1B1- and OATP1B3-mediated transport, pre-incubation with EVR or SIR increased the $K_m$ value (~3–4 folds), with only a slight decrease in or no effect on the $V_{max}$ values of OATP1B1- and OATP1B3, suggesting that pre-incubation with EVR and SIR primarily decreased the affinity of substrates to OATP1B1 and OATP1B3 (Fig. 4 and Table 3). These results were similar to a previous report that CsA-pre-incubation markedly increased the $K_m$ values, rather than the $V_{max}$ for OATP1B1[77]. Without pre-incubation, 5 μM EVR or SIR increased apparent $K_m$ values of OATP1B1 by 6–10 fold, while it had minimal effect (1.2–1.7 fold vs. CTL) on $V_{max}$ values (Supplemental Fig. S6), suggesting that the inhibition of OATP1B1 and OATP1B3 by EVR and SIR following co-incubation most likely occurs in a competitive manner.

In our previous study, pre-incubation with the protein kinase C activator PMA caused a rapid reduction of OATP1B3-mediated transport in association with increased phosphorylation of OATP1B3 [34], suggesting that altered phosphorylation by kinase modulators is likely involved in the rapid reduction of OATP1B1- and OATP1B3-mediated transport after pre-incubation. Among the mTOR phosphorylation sites predicted by the PPSP software, after excluding the sites located in the transmembrane domain predicted by TopPred software[78], four amino acids on OATP1B1 (T10, T186, S194, S682) and five amino acids on OATP1B3 (T10, T186, S194, T656, S683) were predicted sites that can be phosphorylated by the

mTOR kinase. We tested whether inhibition of mTOR kinase activity is a prerequisite for EVR and SIR to exert the preincubation-induced inhibitory effects on OATP1B1- and OATP1B3-mediated transport. INK-128 is a dual inhibitor of mTOR C1 and mTOR C2[79]. In the scenario when both mTOR C1 and C2 kinase activity is inhibited by INK-128 (Fig. 6), EVR and SIR can still exert the preincubation-induced inhibitory effects toward OATP1B1- and OATP1B3-mediated transport (Fig. 7 A and B). These data suggest that the inhibition of mTOR kinase activity is not involved in the inhibitory effects by EVR and SIR preincubation. Among all potential phosphorylation sites identified on OATP1B1 (Table 4), none of these sites was a putative phosphorylation site by the mTOR kinase. This finding may explain why altered mTOR kinase activity is not involved in regulating OATP1B1 and OATP1B3 transport function. The exact mechanism underlying the pre-incubation effects of EVR on OATP1B1- and OATP1B3-mediated transport remains unknown. Several hypotheses, such as trans-inhibition, where inhibition of OATP1B1 and OATP1B3 activity occurs from inside of the cells once the inhibitor enters the cells, and altered post-translational modification (e.g., phosphorylation), have been proposed to explain the pre-incubation-induced reduction of OATP1B1- and 1B3-mediated transport[80]. However, experimental data proving these hypotheses are not available. Mechanistic studies elucidating the pre-incubation-induced reduction in OATP1B1- and OATP1B3-mediated transport will expand our understanding of OATP-mediated DDIs, and warrant further investigation.

In conclusion, the current study reports that pre-incubation with mTOR inhibitors EVR and SIR potentiates the inhibitory effect toward OATP1B1 and OATP1B3 independent of their mTOR inhibition activity, and that these two clinically important immunosuppressants have low potential to cause OATP1B1- and OATP1B3-mediated DDIs.

## Supplementary Material

Refer to Web version on PubMed Central for supplementary material.

## Acknowledgements

We thank Dr. Dietrich Keppler for providing the HEK293-OATP1B1, HEK293-OATP1B3 and HEK293-Mock stable cell lines. We thank Wendy Wang for preparing the samples for LC-MS/MS data collection.

This research was supported by NIH R01 GM094268 [W. Y]. The Q-Exactive Plus mass spectrometer was funded in part by NIH SIG from the Office of The Director, National Institute of Health under Award Number (S10OD018034). The content is solely the responsibility of the authors and does not necessarily represent the official views of the National Institutes of Health. Alexandra Crowe is an American Foundation of Pharmaceutical Education Fellow.

## Abbreviations:

| | |
|---|---|
| **AUC** | area under the plasma concentration-time curve |
| **CsA** | cyclosporine A |
| **DDI** | drug-drug interaction |
| **DMEM** | Dulbecco's Modified Eagle's Medium |

| | |
|---|---|
| **DMSO** | dimethyl sulfoxide |
| **$E_1S$** | estrone sulfate |
| **EVR** | everolimus |
| **FBS** | fetal bovine serum |
| **HBSS** | Hanks' Balanced Salt Solution |
| **$IC_{50}$** | inhibitor concentration producing 50% inhibition |
| **$K_i$** | inhibition constant |
| **mTOR** | mammalian target of rapamycin |
| **OATP** | organic anion-transporting polypeptide |
| **PBPK** | physiologically based pharmacokinetic modeling |
| **SIR** | sirolimus |

## References


1. König J 2010 Uptake transporters of the human OATP family: molecular characteristics, substrates, their role in drug-drug interactions, and functional consequences of polymorphisms. Handbook of experimental pharmacology (201):1–28. [PubMed: 20020358]
2. Shitara Y, Itoh T, Sato H, Li AP, Sugiyama Y 2003 Inhibition of transporter-mediated hepatic uptake as a mechanism for drug-drug interaction between cerivastatin and cyclosporin A. The Journal of pharmacology and experimental therapeutics 304(2):610–616. [PubMed: 12538813]
3. Search Collaborative Group, Link E, Parish S, Armitage J, Bowman L, Heath S, Matsuda F, Gut I, Lathrop M, Collins R 2008 SLCO1B1 variants and statin-induced myopathy--a genomewide study. N Engl J Med 359(8):789–799. [PubMed: 18650507]
4. Vaidyanathan J, Yoshida K, Arya V, Zhang L 2016 Comparing Various In Vitro Prediction Criteria to Assess the Potential of a New Molecular Entity to Inhibit Organic Anion Transporting Polypeptide 1B1. J Clin Pharmacol 56 Suppl 7:S59–72. [PubMed: 27385179]
5. US FDA. 2017 In Vitro Metabolism and Transporter Mediated Drug-Drug Interaction Studies Guidance for Industry. In (CDER) USDoHaHSCfDEaR, editor, ed., Silver Spring, MD: Office of Communications, Division of Drug Information Center for Drug Evaluation and Research Food and Drug Administration.
6. European Medicines Agency. 2012 Guideline on the investigation of drug interactions ed., London, United Kingdom: Committee for Human Medicinal Products (CHMP),.
7. Izumi S, Nozaki Y, Maeda K, Komori T, Takenaka O, Kusuhara H, Sugiyama Y 2015 Investigation of the impact of substrate selection on in vitro organic anion transporting polypeptide 1B1 inhibition profiles for the prediction of drug-drug interactions. Drug Metab Dispos 43(2):235–247. [PubMed: 25414411]
8. Pahwa S, Alam K, Crowe A, Farasyn T, Neuhoff S, Hatley O, Ding K, Yue W 2017 Pretreatment With Rifampicin and Tyrosine Kinase Inhibitor Dasatinib Potentiates the Inhibitory Effects Toward OATP1B1- and OATP1B3-Mediated Transport. J Pharm Sci 106(8):2123–2135. [PubMed: 28373111]
9. Gertz M, Cartwright CM, Hobbs MJ, Kenworthy KE, Rowland M, Houston JB, Galetin A 2013 Cyclosporine inhibition of hepatic and intestinal CYP3A4, uptake and efflux transporters: application of PBPK modeling in the assessment of drug-drug interaction potential. Pharm Res 30(3):761–780. [PubMed: 23179780]

10. Yoshikado T, Yoshida K, Kotani N, Nakada T, Asaumi R, Toshimoto K, Maeda K, Kusuhara H, Sugiyama Y 2016 Quantitative Analyses of Hepatic OATP-Mediated Interactions Between Statins and Inhibitors Using PBPK Modeling With a Parameter Optimization Method. Clin Pharmacol Ther 100(5):513–523. [PubMed: 27170342]
11. Wyeth-Ayerst Pharmaceuticals Inc. 2000 Rapamune (sirolimus) Package Insert ed., Philadelphia, PA.
12. Novartis. 2010 Zortress® (everolimus) tablets prescribing information ed., East Hanover, NJ.
13. Benjamin D, Colombi M, Moroni C, Hall MN 2011 Rapamycin passes the torch: a new generation of mTOR inhibitors. Nature reviews Drug discovery 10(11):868–880. [PubMed: 22037041]
14. Faivre S, Kroemer G, Raymond E 2006 Current development of mTOR inhibitors as anticancer agents. Nature reviews Drug discovery 5(8):671–688. [PubMed: 16883305]
15. Zaytseva YY, Valentino JD, Gulhati P, Evers BM 2012 mTOR inhibitors in cancer therapy. Cancer letters 319(1):1–7. [PubMed: 22261336]
16. Novartis. 2009 Afinitor® (everolimus) tablets prescribing information ed., East Hanover, NJ.
17. Aakhus S, Dahl K, Widerøe TE 1999 Cardiovascular morbidity and risk factors in renal transplant patients. Nephrology Dialysis Transplantation 14:648–654.
18. Ritz E, Wanner C 2008 Statin use prolongs patient survival after renal transplantation. J Am Soc Nephrol 19(11):2037–2040. [PubMed: 18842988]
19. Milowsky MI, Iyer G, Regazzi AM, Al-Ahmadie H, Gerst SR, Ostrovnaya I, Gellert LL, Kaplan R, Garcia-Grossman IR, Pendse D, Balar AV, Flaherty AM, Trout A, Solit DB, Bajorin DF 2013 Phase II study of everolimus in metastatic urothelial cancer. BJU Int 112(4):462–470. [PubMed: 23551593]
20. Donders F, Kuypers D, Wolter P, Neven P 2014 Everolimus in acute kidney injury in a patient with breast cancer: a case report. J Med Case Rep 8:386. [PubMed: 25420955]
21. Barshes NR, Goodpastor SE, Goss JA 2003 Sirolimus-atorvastatin drug interaction in the pancreatic islet transplant recipient. Transplantation 76(11):1649–1650. [PubMed: 14702546]
22. Hong YA, Kim HD, Jo K, Park YK, Lee J, Sun IO, Chung BH, Park CW, Yang CW, Choi BS 2014 Severe rhabdomyolysis associated with concurrent use of simvastatin and sirolimus after cisplatin-based chemotherapy in a kidney transplant recipient. Experimental and clinical transplantation : official journal of the Middle East Society for Organ Transplantation 12(2):152–155. [PubMed: 23734754]
23. Pasanen MK, Fredrikson H, Neuvonen PJ, Niemi M 2007 Different effects of SLCO1B1 polymorphism on the pharmacokinetics of atorvastatin and rosuvastatin. Clinical pharmacology and therapeutics 82(6):726–733. [PubMed: 17473846]
24. Picard N, Levoir L, Lamoureux F, Yee SW, Giacomini KM, Marquet P 2011 Interaction of sirolimus and everolimus with hepatic and intestinal organic anion-transporting polypeptide transporters. Xenobiotica; the fate of foreign compounds in biological systems 41(9):752–757. [PubMed: 21524191]
25. Loewith R, Jacinto E, Wullschleger S, Lorberg A, Crespo JL, Bonenfant D, Oppliger W, Jenoe P, Hall MN 2002 Two TOR Complexes, Only One of which Is Rapamycin Sensitive, Have Distinct Roles in Cell Growth Control. Molecular cell 10:457–468. [PubMed: 12408816]
26. Bhagwat SV, Gokhale PC, Crew AP, Cooke A, Yao Y, Mantis C, Kahler J, Workman J, Bittner M, Dudkin L, Epstein DM, Gibson NW, Wild R, Arnold LD, Houghton PJ, Pachter JA 2011 Preclinical characterization of OSI-027, a potent and selective inhibitor of mTORC1 and mTORC2: distinct from rapamycin. Mol Cancer Ther 10(8):1394–1406. [PubMed: 21673091]
27. Lou HZ, Weng XC, Pan HM, Pan Q, Sun P, Liu LL, Chen B 2014 The novel mTORC½ dual inhibitor INK-128 suppresses survival and proliferation of primary and transformed human pancreatic cancer cells. Biochem Biophys Res Commun 450(2):973–978. [PubMed: 24971544]
28. Xue Y, Li A, Wang L, Feng H, Yao X 2006 PPSP: prediction of PK-specific phosphorylation site with Bayesian decision theory. BMC Bioinformatics 7:163. [PubMed: 16549034]
29. Alam K, Farasyn T, Crowe A, Ding K, Yue W 2017 Treatment with proteasome inhibitor bortezomib decreases organic anion transporting polypeptide (OATP) 1B3-mediated transport in a substrate-dependent manner. PLoS One 12(11):e0186924. [PubMed: 29107984]

30. König J, Cui Y, Nies AT, Keppler D 2000 Localization and genomic organization of a new hepatocellular organic anion transporting polypeptide. J Biol Chem 275(30):23161–23168. [PubMed: 10779507]
31. Konig J, Cui Y, Nies AT, Keppler D 2000 A novel human organic anion transporting polypeptide localized to the basolateral hepatocyte membrane. Am J Physiol Gastrointest Liver Physiol 278(1):G156–164. [PubMed: 10644574]
32. Alam K, Pahwa S, Wang X, Zhang P, Ding K, Abuznait AH, Li L, Yue W 2016 Downregulation of Organic Anion Transporting Polypeptide (OATP) 1B1 Transport Function by Lysosomotropic Drug Chloroquine: Implication in OATP-Mediated Drug-Drug Interactions. Molecular Pharmaceutics 13(3):839–851. [PubMed: 26750564]
33. Pahwa S, Alam K, Crowe A, Farasyn T, Neuhoff S, Hatley O, Ding K, Yue W 2017 Pretreatment With Rifampicin and Tyrosine Kinase Inhibitor Dasatinib Potentiates the Inhibitory Effects Toward OATP1B1- and OATP1B3-Mediated Transport. J Pharm Sci 106:2123–2135. [PubMed: 28373111]
34. Powell J, Farasyn T, Kock K, Meng X, Pahwa S, Brouwer KL, Yue W 2014 Novel mechanism of impaired function of organic anion-transporting polypeptide 1B3 in human hepatocytes: post-translational regulation of OATP1B3 by protein kinase C activation. Drug Metab Dispos 42(11): 1964–1970. [PubMed: 25200870]
35. Hirano M, Maeda K, Shitara Y, Sugiyama Y 2004 Contribution of OATP2 (OATP1B1) and OATP8 (OATP1B3) to the hepatic uptake of pitavastatin in humans. J Pharmacol Exp Ther 311(1):139–146. [PubMed: 15159445]
36. Kitamura S, Maeda K, Wang Y, Sugiyama Y 2008 Involvement of multiple transporters in the hepatobiliary transport of rosuvastatin. Drug Metab Dispos 36(10):2014–2023. [PubMed: 18617601]
37. Bradley SE, Ingelfinger FJ, et al. 1945 The estimation of hepatic blood flow in man. The Journal of clinical investigation 24:890–897.
38. US FDA. 2009 Everolimus Clinical Pharmacology and Biopharmaceutics Review. In Research CfDEa, editor, ed.: Center for Drug Evaluation and Research Office of Clinical Pharmacology.
39. Emoto C, Fukuda T, Cox S, Christians U, Vinks AA 2013 Development of a Physiologically-Based Pharmacokinetic Model for Sirolimus: Predicting Bioavailability Based on Intestinal CYP3A Content. CPT Pharmacometrics Syst Pharmacol 2:e59. [PubMed: 23884207]
40. ACD/Structure Elucidator. 2017 version 15.01 ed., Toronto, On, Canada: Advanced Chemistry Development, Inc.
41. Mano Y, Sugiyama Y, Ito K 2015 Use of a Physiologically Based Pharmacokinetic Model for Quantitative Prediction of Drug-Drug Interactions via CYP3A4 and Estimation of the Intestinal Availability of CYP3A4 Substrates. J Pharm Sci 104(9):3183–3193. [PubMed: 26045365]
42. Kovarik JM, Kahan BD, Kaplan B, Lorber M, Winkler M, Rouilly M, Gerbeau C, Cambon N, Boger R, Rordorf C, Everolimus Phase 2 Study G 2001 Longitudinal assessment of everolimus in de novo renal transplant recipients over the first post-transplant year: pharmacokinetics, exposure-response relationships, and influence on cyclosporine. Clinical pharmacology and therapeutics 69(1):48–56. [PubMed: 11180038]
43. Jamei M, Turner D, Yang J, Neuhoff S, Polak S, Rostami-Hodjegan A, Tucker G 2009 Population-based mechanistic prediction of oral drug absorption. AAPS J 11(2):225–237. [PubMed: 19381840]
44. Pade D, Jamei M, Rostami-Hodjegan A, Turner DB 2017 Application of the MechPeff model to predict passive effective intestinal permeability in the different regions of the rodent small intestine and colon. Biopharmaceutics & drug disposition 38(2):94–114. [PubMed: 28214380]
45. European Medicines Agency. 2014 Afinitor (everolimus) Summary of Product Characteristics ed., London, United Kingdom.
46. Crowe A, Lemaire M 1998 In vitro and in situ absorption of SDZ-RAD using a human intestinal cell line (Caco-2) and a single pass perfusion model in rats: comparison with rapamycin. Pharm Res 15:1666–1672. [PubMed: 9833985]
47. Kenny JR, Mukadam S, Zhang C, Tay S, Collins C, Galetin A, Khojasteh SC 2012 Drug-drug interaction potential of marketed oncology drugs: in vitro assessment of time-dependent

cytochrome P450 inhibition, reactive metabolite formation and drug-drug interaction prediction. Pharm Res 29(7):1960–1976. [PubMed: 22415140]

48. Patki KC, Von Moltke LL, Greenblatt DJ 2003 In vitro metabolism of midazolam, triazolam, nifedipine, and testosterone by human liver microsomes and recombinant cytochromes p450: role of cyp3a4 and cyp3a5. Drug Metab Dispos 31(7):938–944. [PubMed: 12814972]
49. Urva S, Bouillaud E, Delaney R, Jappe A, Cheung W 2013 A phase I study evaluating the effect of everolimus on the pharmacokinetics of midazolam in healthy subjects. J Clin Pharmacol 53(4): 444–450. [PubMed: 23426978]
50. Jacobsen W, Kirchner G, Hallensleben K, Mancinelli L, Deters M, Hackbarth I, Benet LZ, Sewing KF, Christians U 1999 Comparison of cytochrome P-450-dependent metabolism and drug interactions of the 3-hydroxy-3-methylglutaryl-CoA reductase inhibitors lovastatin and pravastatin in the liver. Drug Metab Dispos 27(2):173–179. [PubMed: 9929499]
51. Nozawa T, Imai K, Nezu J, Tsuji A, Tamai I 2004 Functional characterization of pH-sensitive organic anion transporting polypeptide OATP-B in human. J Pharmacol Exp Ther 308(2):438–445. [PubMed: 14610227]
52. Shirasaka Y, Suzuki K, Nakanishi T, Tamai I 2010 Intestinal absorption of HMG-CoA reductase inhibitor pravastatin mediated by organic anion transporting polypeptide. Pharm Res 27(10):2141–2149. [PubMed: 20686826]
53. Watanabe T, Kusuhara H, Maeda K, Shitara Y, Sugiyama Y 2009 Physiologically based pharmacokinetic modeling to predict transporter-mediated clearance and distribution of pravastatin in humans. J Pharmacol Exp Ther 328(2):652–662. [PubMed: 19001154]
54. Shirasaka Y, Suzuki K, Nakanishi T, Tamai I 2011 Differential effect of grapefruit juice on intestinal absorption of statins due to inhibition of organic anion transporting polypeptide and/or P-glycoprotein. J Pharm Sci 100(9):3843–3853. [PubMed: 21520088]
55. Shitara Y, Sugiyama Y 2006 Pharmacokinetic and pharmacodynamic alterations of 3-hydroxy-3-methylglutaryl coenzyme A (HMG-CoA) reductase inhibitors: drug-drug interactions and interindividual differences in transporter and metabolic enzyme functions. Pharmacol Ther 112(1): 71–105. [PubMed: 16714062]
56. Wojtal KA, Eloranta JJ, Hruz P, Gutmann H, Drewe J, Staumann A, Beglinger C, Fried M, Kullak-Ublick GA, Vavricka SR 2009 Changes in mRNA expression levels of solute carrier transporters in inflammatory bowel disease patients. Drug Metab Dispos 37(9):1871–1877. [PubMed: 19487253]
57. Meier Y, Eloranta JJ, Darimont J, Ismair MG, Hiller C, Fried M, Kullak-Ublick GA, Vavricka SR 2007 Regional distribution of solute carrier mRNA expression along the human intestinal tract. Drug Metab Dispos 35(4):590–594. [PubMed: 17220238]
58. Hilgendorf C, Ahlin G, Seithel A, Artursson P, Ungell AL, Karlsson J 2007 Expression of thirty-six drug transporter genes in human intestine, liver, kidney, and organotypic cell lines. Drug Metab Dispos 35(8):1333–1340. [PubMed: 17496207]
59. Groer C, Bruck S, Lai Y, Paulick A, Busemann A, Heidecke CD, Siegmund W, Oswald S 2013 LC-MS/MS-based quantification of clinically relevant intestinal uptake and efflux transporter proteins. J Pharm Biomed Anal 85:253–261. [PubMed: 23973632]
60. Miyauchi E, Tachikawa M, Decleves X, Uchida Y, Bouillot JL, Poitou C, Oppert JM, Mouly S, Bergmann JF, Terasaki T, Scherrmann JM, Lloret-Linares C 2016 Quantitative Atlas of Cytochrome P450, UDP-Glucuronosyltransferase, and Transporter Proteins in Jejunum of Morbidly Obese Subjects. Mol Pharm 13(8):2631–2640. [PubMed: 27347605]
61. Drozdzik M, Groer C, Penski J, Lapczuk J, Ostrowski M, Lai Y, Prasad B, Unadkat JD, Siegmund W, Oswald S 2014 Protein abundance of clinically relevant multidrug transporters along the entire length of the human intestine. Mol Pharm 11(10):3547–3555. [PubMed: 25158075]
62. Zimmerman JJ, Kahan BD 1997 Pharmacokinetics of Sirolimus in Stable Renal Transplant Patients after Multiple Dose Administration. Journal of Clinical Pharmacology 37:405–415. [PubMed: 9156373]
63. Yoshikado T, Yoshida K, Kotani N, Nakada T, Asaumi R, Toshimoto K, Maeda K, Kusuhara H, Sugiyama Y 2016 Quantitative Analyses of Hepatic OATP-Mediated Interactions Between Statins and Inhibitors Using PBPK Modeling With a Parameter Optimization Method. Clinical pharmacology and therapeutics

64. Brattstrom C, Sawe J, Jansson B, Lonnebo A, Nordin J, Zimmerman JJ, Burke JT, Groth CG 2000 Pharmacokinetics and Safety of Single Oral Doses of Sirolimus (Rapamycin) in Healthy Male Volunteers. Therapeutic Drug Monitoring 22:537–544. [PubMed: 11034258]
65. Nojima H, Tokunaga C, Eguchi S, Oshiro N, Hidayat S, Yoshino K, Hara K, Tanaka N, Avruch J, Yonezawa K 2003 The mammalian target of rapamycin (mTOR) partner, raptor, binds the mTOR substrates p70 S6 kinase and 4E-BP1 through their TOR signaling (TOS) motif. J Biol Chem 278(18):15461–15464. [PubMed: 12604610]
66. Moschella PC, McKillop J, Pleasant DL, Harston RK, Balasubramanian S, Kuppuswamy D 2013 mTOR complex 2 mediates Akt phosphorylation that requires PKCepsilon in adult cardiac muscle cells. Cell Signal 25(9):1904–1912. [PubMed: 23673367]
67. Breuleux M, Klopfenstein M, Stephan C, Doughty CA, Barys L, Maira SM, Kwiatkowski D, Lane HA 2009 Increased AKT S473 phosphorylation after mTORC1 inhibition is rictor dependent and does not predict tumor cell response to PI3K/mTOR inhibition. Mol Cancer Ther 8(4):742–753. [PubMed: 19372546]
68. Matrix Science Inc. 2016 Scoring: Mascot Probability Based Scoring. Mascot database help search, ed.
69. Taus T, Kocher T, Pichler P, Paschke C, Schmidt A, Henrich C, Mechtler K 2011 Universal and confident phosphorylation site localization using phosphoRS. J Proteome Res 10(12):5354–5362. [PubMed: 22073976]
70. Robertsen I, Asberg A, Granseth T, Vethe NT, Akhlaghi F, Ghareeb M, Molden E, Reier-Nilsen M, Holdaas H, Midtvedt K 2014 More potent lipid-lowering effect by rosuvastatin compared with fluvastatin in everolimus-treated renal transplant recipients. Transplantation 97(12):1266–1271. [PubMed: 24521776]
71. Martin PD, Warwick MJ, Dane AL, Cantarini MV 2003 A Double-Blind, Randomized, Incomplete Crossover Trial to Assess the Dose Proportionality of Rosuvastatin in HealthyVolunteers. Clinical Therapeutics 23(8):2215–2224.
72. Dopazo C, Bilbao I, Lázaro JL, Sapisochin G, Caralt M, Blanco L, Castells L, Charco R 2009 Severe rhabdomyolysis and acute renal failure secondary to concomitant use of simvastatin with rapamycin plus tacrolimus in liver transplant patient. Transplantation proceedings 41(3):1021–1024. [PubMed: 19376416]
73. Basic-Jukic N, Kes P, Bubic-Filipi L, Vranjican Z 2010 Rhabdomyolysis and acute kidney injury secondary to concomitant use of fluvastatin and rapamycin in a renal transplant recipient. Nephrology, dialysis, transplantation : official publication of the European Dialysis and Transplant Association - European Renal Association 25(6):7.
74. Ishigam M, Uchiyama M, Kondo T, Iwabuchi H, Inoue S, Takasaki W, Ikeda T, Komai T, Ito K, Sugiyama Y 2001 Inhibition of in vitro metabolism of simvastatin by itraconazole in humans and prediction of in vivo drug-drug interactions. Pharm Res 18(5):622–631. [PubMed: 11465417]
75. Fischer V, Johanson L, Heitz F, Tullman R, Graham E, Baldeck JP, Robinson WT 1999 The 3-hydroxy-3-methylglutaryl coenzyme A reductase inhibitor fluvastatin: effect on human cytochrome P-450 and implications for metabolic drug interactions. Drug Metab Dispos 27(3): 410–416. [PubMed: 10064574]
76. Lampen A, Christians U, Bader A, Hackbarth I, Sewing KF 1996 Drug interactions and interindividual variability of ciclosporin metabolism in the small intestine. Pharmacology 52(3): 159–168. [PubMed: 8849485]
77. Shitara Y, Takeuchi K, Nagamatsu Y, Wada S, Sugiyama Y, Horie T 2012 Long-lasting Inhibitory Effects of Cyclosporin A, but Not Tacrolimus, on OATP1B1- and OATP1B3-mediated Uptake. Drug Metab Pharmacokinet 27(4):368–378. [PubMed: 22240838]
78. Gv Heijne 1992 Membrane Protein Structure Prediction Hydrophobicity Analysis and the Positive-inside Rule. Journal of Molecular Biology 225:487–494. [PubMed: 1593632]
79. Liu Q, Thoreen C, Wang J, Sabatini D, Gray NS 2009 mTOR Mediated Anti-Cancer Drug Discovery. Drug Discov Today Ther Strateg 6(2):47–55. [PubMed: 20622997]
80. Shitara Y, Sugiyama Y 2017 Preincubation-dependent and long-lasting inhibition of organic anion transporting polypeptide (OATP) and its impact on drug-drug interactions. Pharmacol Ther 177:67–80. [PubMed: 28249706]

81. Afinitor. 2009 Package insert ed., Novartis, East Hanover, NJ.
82. Hsieh Y, Galviz G, Long BJ 2009 Ultra-performance hydrophilic interaction liquid chromatography/tandem mass spectrometry for the determination of everolimus in mouse plasma. Rapid Commun Mass Spectrom 23(10):1461–1466. [PubMed: 19350527]
83. Kovarik JM, Hsu CH, McMahon L, Berthier S, Rordorf C 2001 Population pharmacokinetics of everolimus in de novo renal transplant patients: impact of ethnicity and comedications. Clinical pharmacology and therapeutics 70(3):247–254. [PubMed: 11557912]
84. Matrix Science Inc. 2016 Scoring: Mascot Probability Based Scoring. In search Mdh, editor, ed.
85. Brenton AG, Godfrey AR 2010 Accurate mass measurement: terminology and treatment of data. J Am Soc Mass Spectrom 21(11):1821–1835. [PubMed: 20650651]

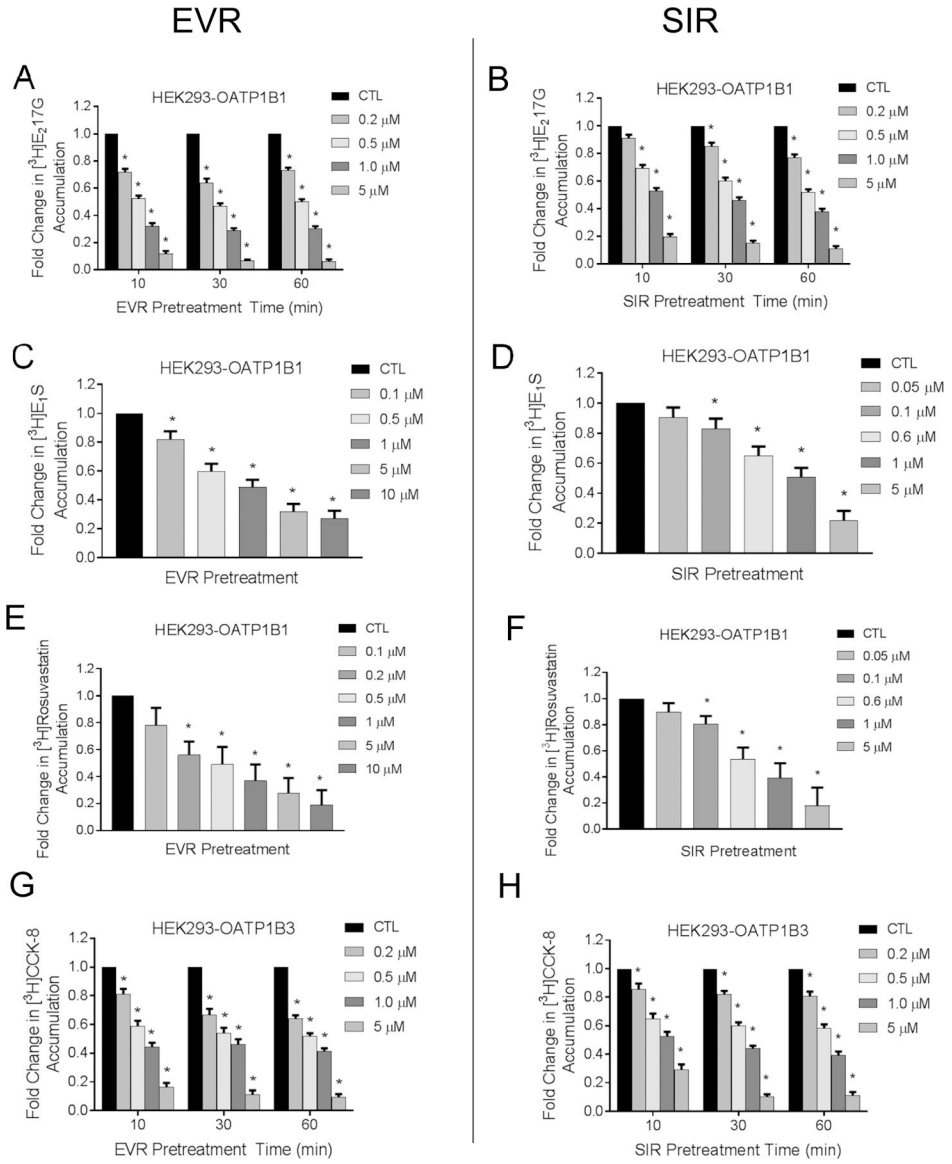


**Fig. 1. Effects of pre-incubation with EVR and SIR on OATP1B1- and OATP1B3-mediated transport.**

Model-estimated fold change and associated SE of the accumulation of [$^3$H]-$E_2$17βG (1 μM, 2 min) (A-B), [$^3$H]-$E_1$S (25 nM, 0.5 min) (C-D), [$^3$H]-rosuvastatin (20 nM, 0.5 min) (E-F), and [$^3$H]-CCK-8 (1 μM, 3 min) (G-H) vs. CTL in HEK293-OATP1B1 and HEK293-OATP1B3 cells after pre-incubation with 0.1 – 10 μM EVR or 0.05 – 5 μM SIR for 10 min, 30 min, and 1 hour as indicated in the legend. Substrate accumulation was determined in the absence of EVR or SIR after washing. Linear mixed effects models were fit to the data as described in the “Materials and Methods” (n=3 in triplicate). * indicates a statistically significant difference (Bonferroni-adjusted $p<0.05$) vs. CTL.

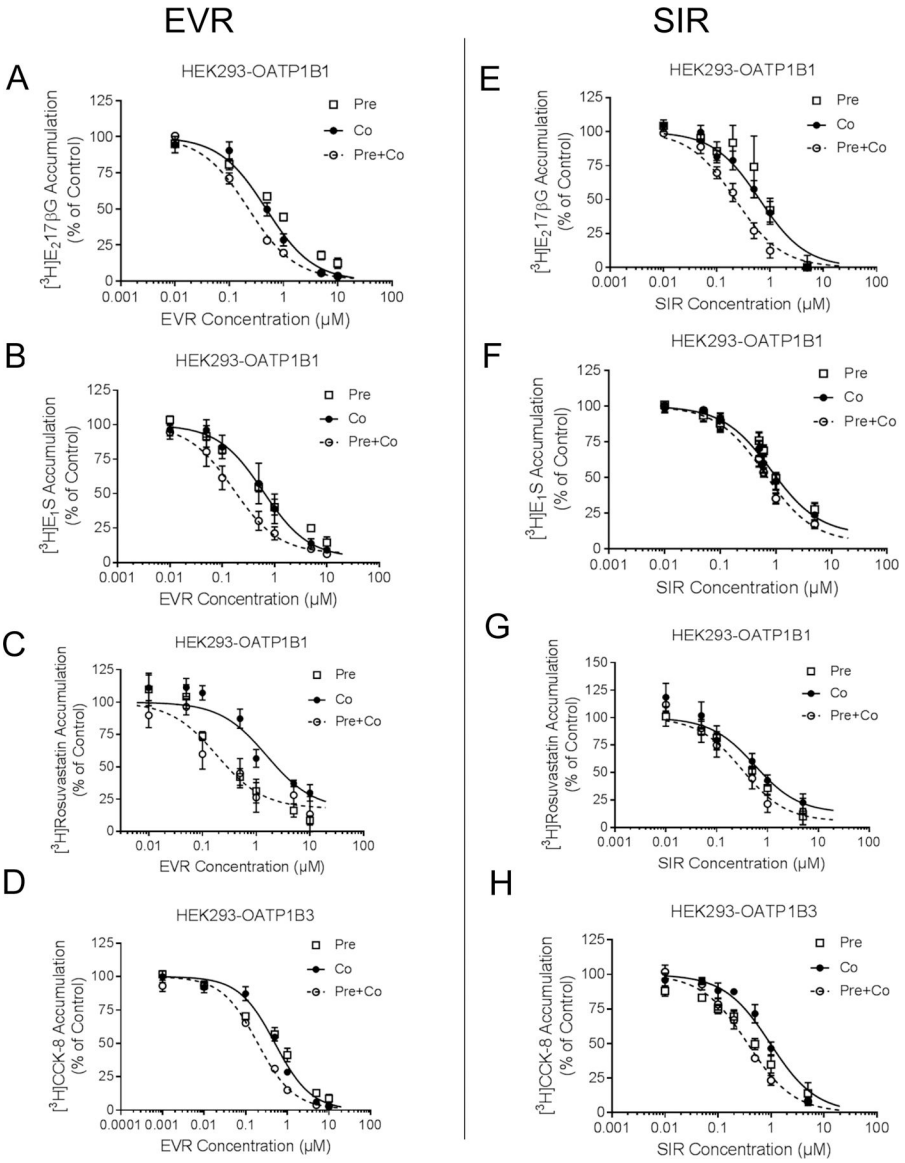


**Fig. 2. Effects of pre-incubation with EVR and SIR on the $IC_{50}$ values against OATP1B1 and OATP1B3.**

OATP1B1- and OATP1B3-mediated transport of [$^3$H]-$E_2$17βG and [$^3$H]-CCK-8 is expressed as percentage of vehicle control in pre-incubation (open squares), co-incubation (closed circles), and pre+co-incubation (open circles) scenarios with 0.001 – 10 μM EVR (A-D) or 0.01 – 5 μM SIR (E-H) as inhibitor as described in the Materials and Methods. Data represent mean ± SE (n=3 in triplicate). The $IC_{50}$ values were determined by fitting dose-response curves to the data by nonlinear regression analysis, and are summarized in Table 1. Solid (co-incubation) and dashed (pre+co-incubation) lines represent the fitted lines.

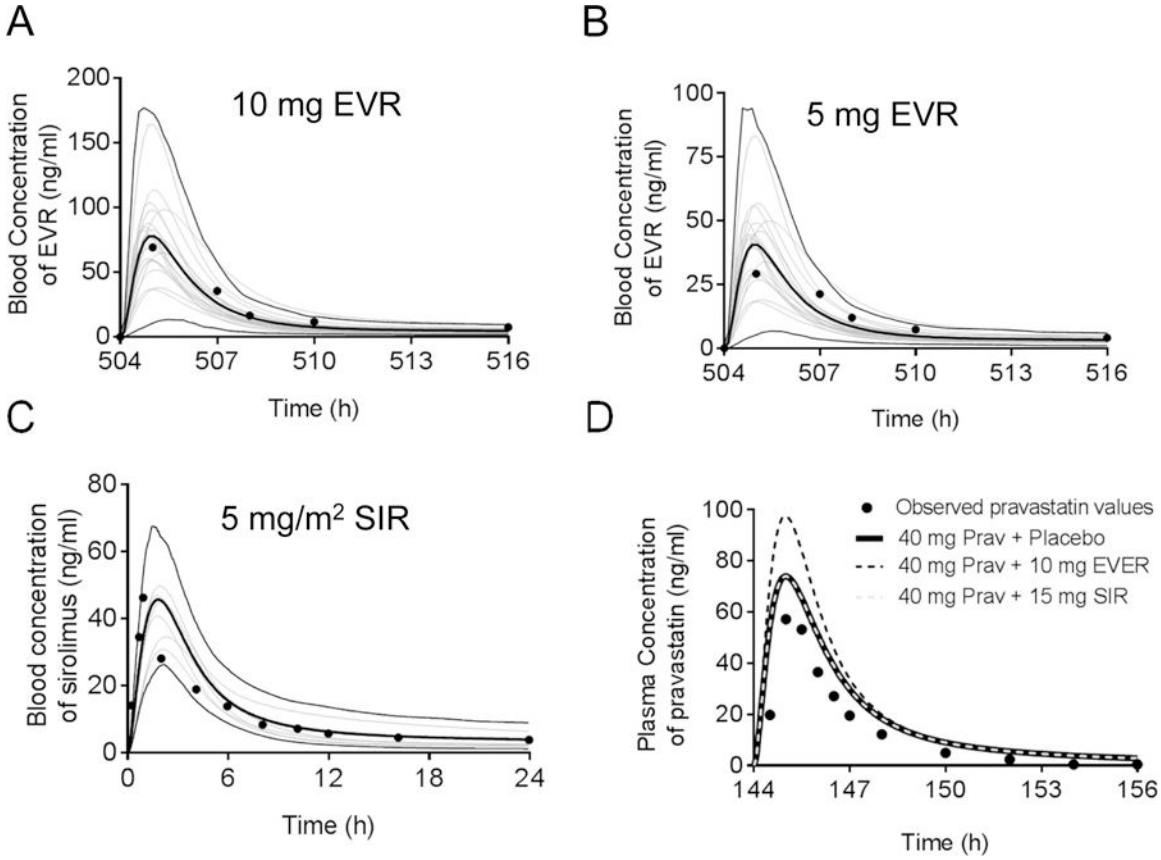


**Fig. 3. Simulated *versus* observed system concentration-time profiles of orally administered EVR, SIR, and pravastatin in healthy volunteers.**

Blood concentration-time profile of EVR (A) 10 mg and (B) 5 mg weekly doses. The grey thin lines represent simulated individual trials (20) of 4 subjects using a population of 80 virtual subjects (50% female, 28–83 years) for figure A and B. The thin black lines represent the upper (95$^{th}$) and lower (5$^{th}$) percentiles, and the thick black line represents the simulated mean values of the healthy volunteers population (n=80). The circles denote mean values from the clinical data from the US FDA, 2009[38]. (C) Blood concentration-time profile of a 5 mg/m$^2$ single dose of SIR. The thin grey lines represent simulated individual trials (10) of 30 male subjects using a population of 300 virtual subjects (19–36 years). The thin black lines represent the upper (95$^{th}$) and lower (5$^{th}$) percentiles, and the thick black line represents the simulated mean values of the healthy volunteers population (n=300). The circles denote mean values from the clinical study by Brattstrom *et al.*, 2000[64]. (D) Simulated *versus* observed plasma concentrations of pravastatin following co-administration of a single dose pravastatin (40 mg) with placebo (black line), EVR (10 mg, black dashed line) or SIR (15 mg, grey dashed line). Lines represent the mean values of simulated virtual populations of 400 healthy volunteers (20 trials X 20 subjects, 50% female, 20–50 years). Note that the pravastatin placebo simulation and the pravastatin-SIR simulation overlap.

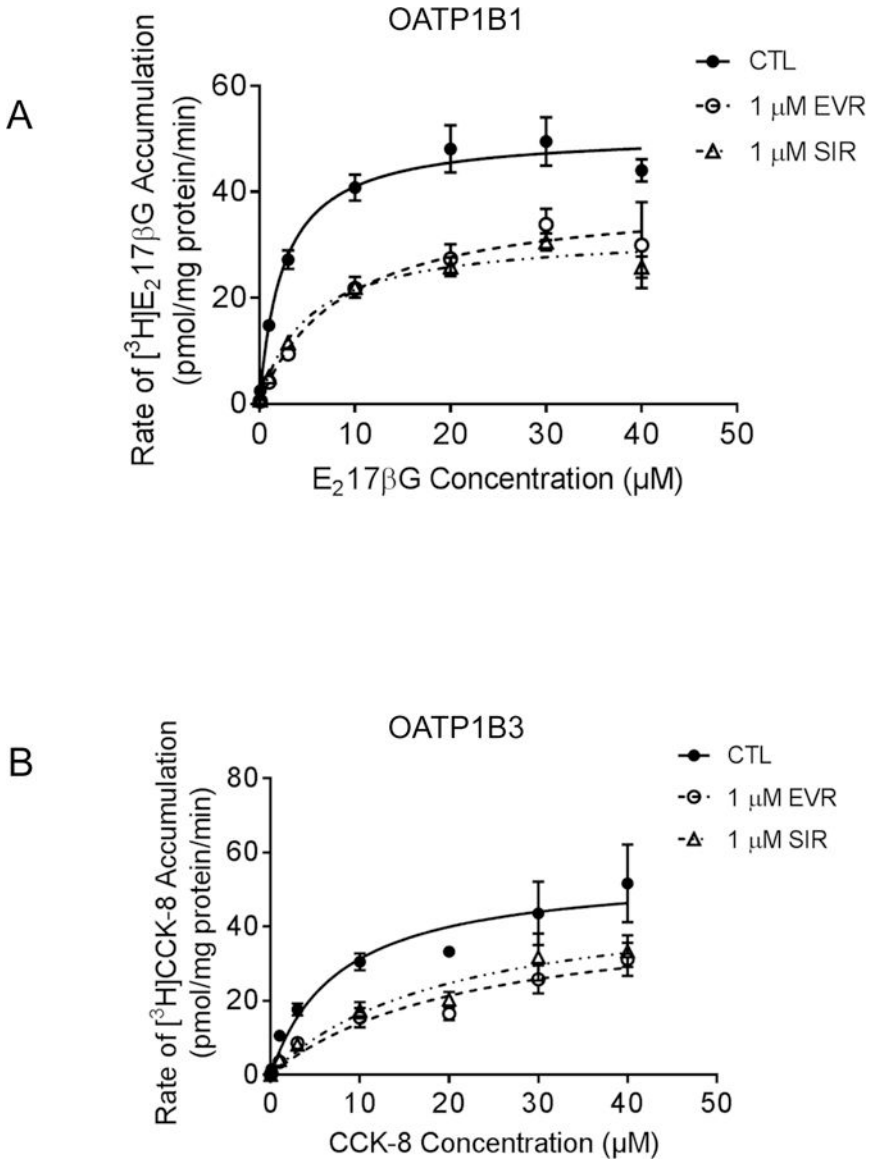


**Fig 4. Effects of EVR and SIR on the kinetic parameters of OATP1B1- and OATP1B3mediated transport.**

The concentration-dependent accumulation of (A) [$^3$H]-$E_2$17βG (0.1–40 μM, 2 min) mediated by OATP1B1 and (B) [$^3$H]-CCK-8 (0.1–40 μM, 3 min)-mediated by OATP1B3 in HEK293-OATP1B1 and –OATP1B3 cells pre-incubated with vehicle CTL, EVR (1 μM, 1 h), or SIR (1 μM, 1 h). Values of [$^3$H]$E_2$17βG accumulation in Mock cells were subtracted from those in HEK293-OATP1B1 cells. $V_{max}$ and $K_m$ values were determined as described in the Material and Methods. Solid, dashed line, and dotted line represent the best fits of the Michaelis–Menten equation to the data of CTL (closed circles), EVR (open circles), or SIR pre-incubation (open triangles), respectively. Data represent the mean ± SD of a representative graph of three and 5 independent experiments for OATP1B1 and OATP1B3, respectively, in triplicate.

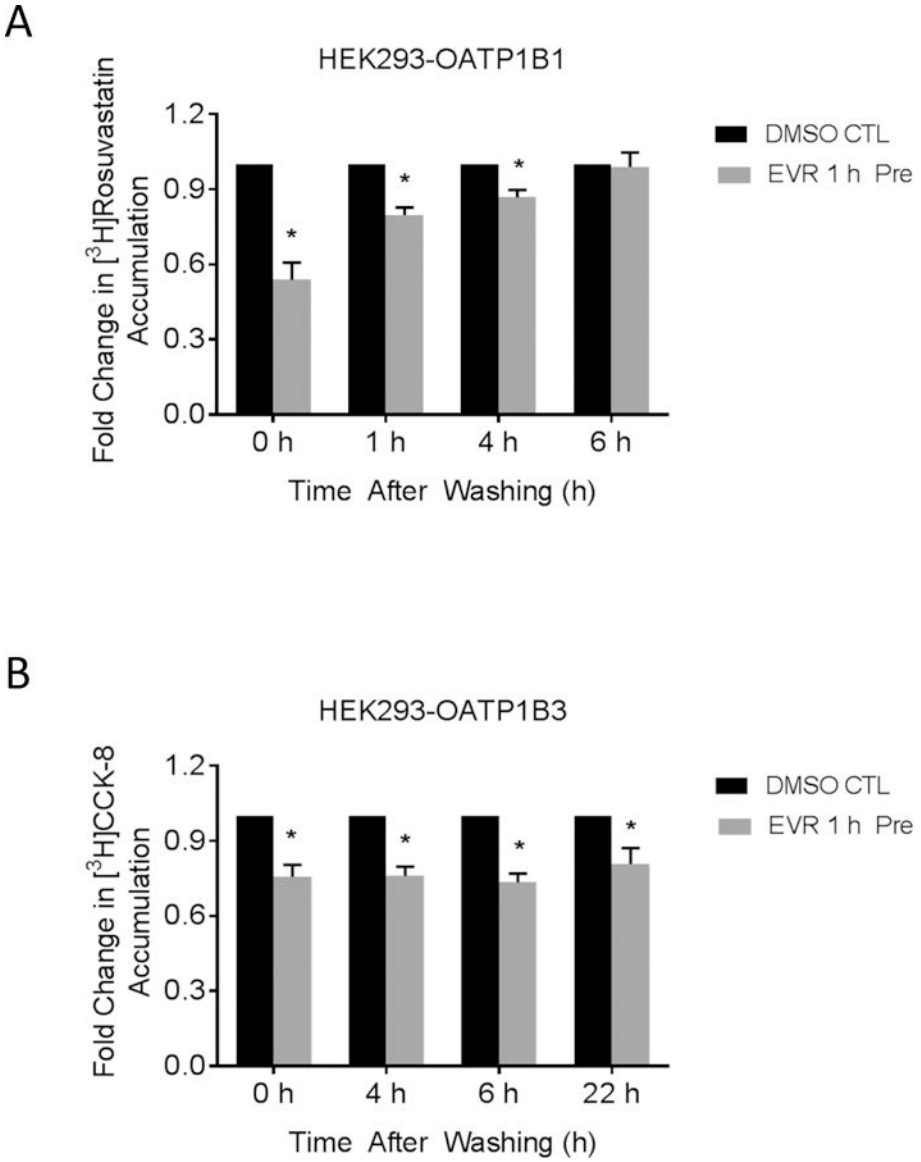


**Fig 5. Long-lasting inhibitory effects of EVR on OATP1B1- and OATP1B3-mediated transport.** Model-estimated fold change and associated *SE* of the accumulation of [$^3$H]-rosuvastatin (20 nM, 0.5 min) (A) and [$^3$H]-CCK-8 (1 μM, 3 min) (B) vs. vehicle control (CTL). HEK293-OATP1B1 or –OATP1B3 cells were pre-incubated with CTL or 0.2 μM EVR-containing culture medium for 1 h. At the end of pre-incubation, the culture medium was removed and cells were washed three times with fresh culture medium and cultured in inhibitor-free medium for the indicated time periods. [$^3$H]-rosuvastatin (20 nM, 0.5 min) (A) or [$^3$H]CCK-8 (1 μM, 3 min) accumulation was determined at the indicated time points ($n$=3 in triplicate) in the absence of EVR after washing. Fold changes and SE were estimated using a generalized linear mixed model, as described in the "Materials and Methods". * indicates a statistically significant difference ($p$<0.05) vs. CTL.

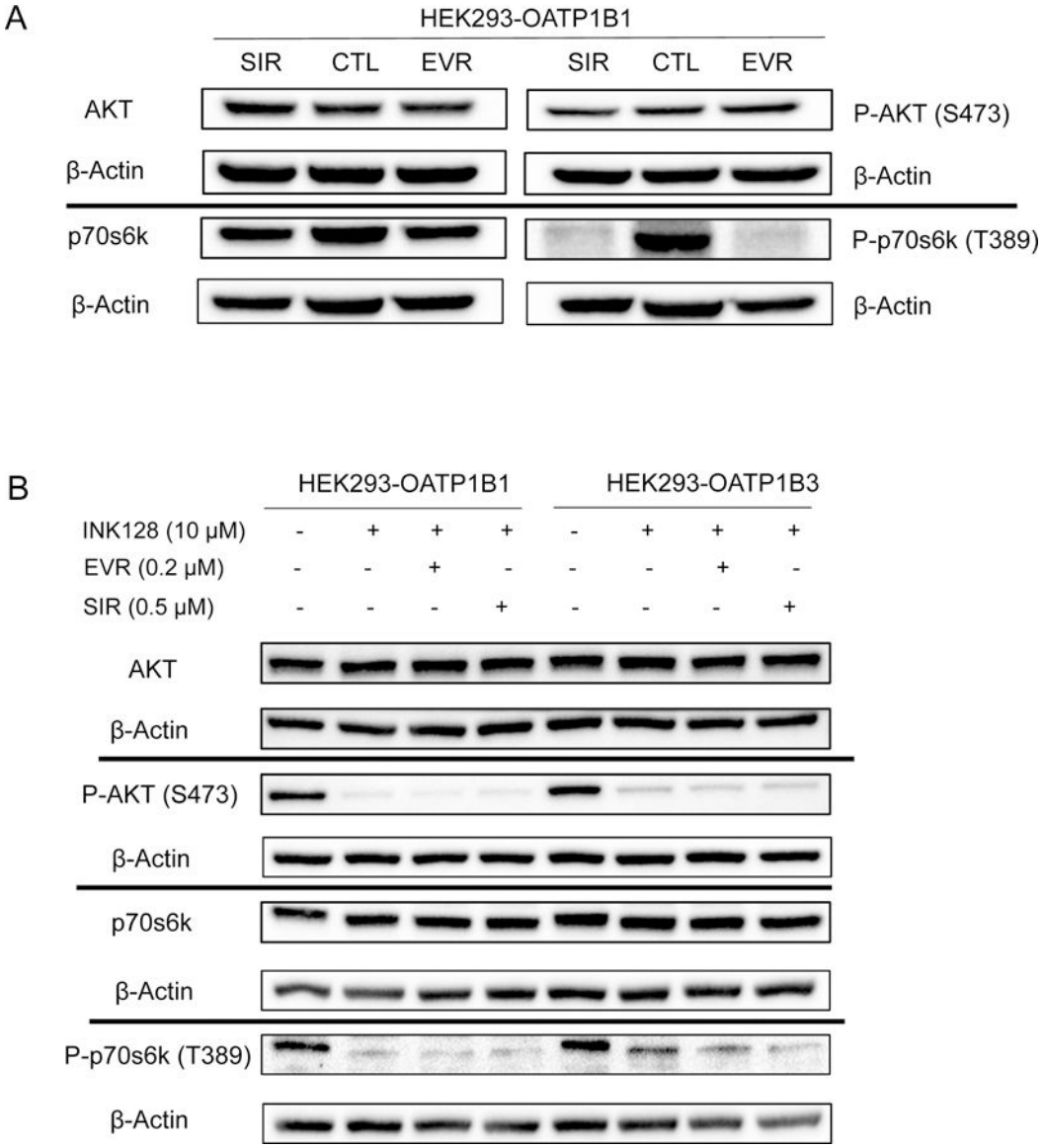


**Fig. 6. Effects of EVR and SIR on the phosphorylation status of mTOR downstream proteins p70s6k and AKT.**

Immunoblot of phosphor-AKT (p-AKT), total AKT, phosphor-p70s6k (p-p70s6k), and total p70s6k in (A) HEK293-OATP1B1 cells after 1 h incubation with 0.2 μM EVR, 0.5 μM SIR, or vehicle control and in (B) HEK293-OATP1B1 and −1B3 cells after 1 h incubation with INK128 (10 μM) alone, or prior to incubation with EVR (0.2 μM, 1 h) or SIR (0.5 μM, 1 h) (representative figures from N=3 experiments).

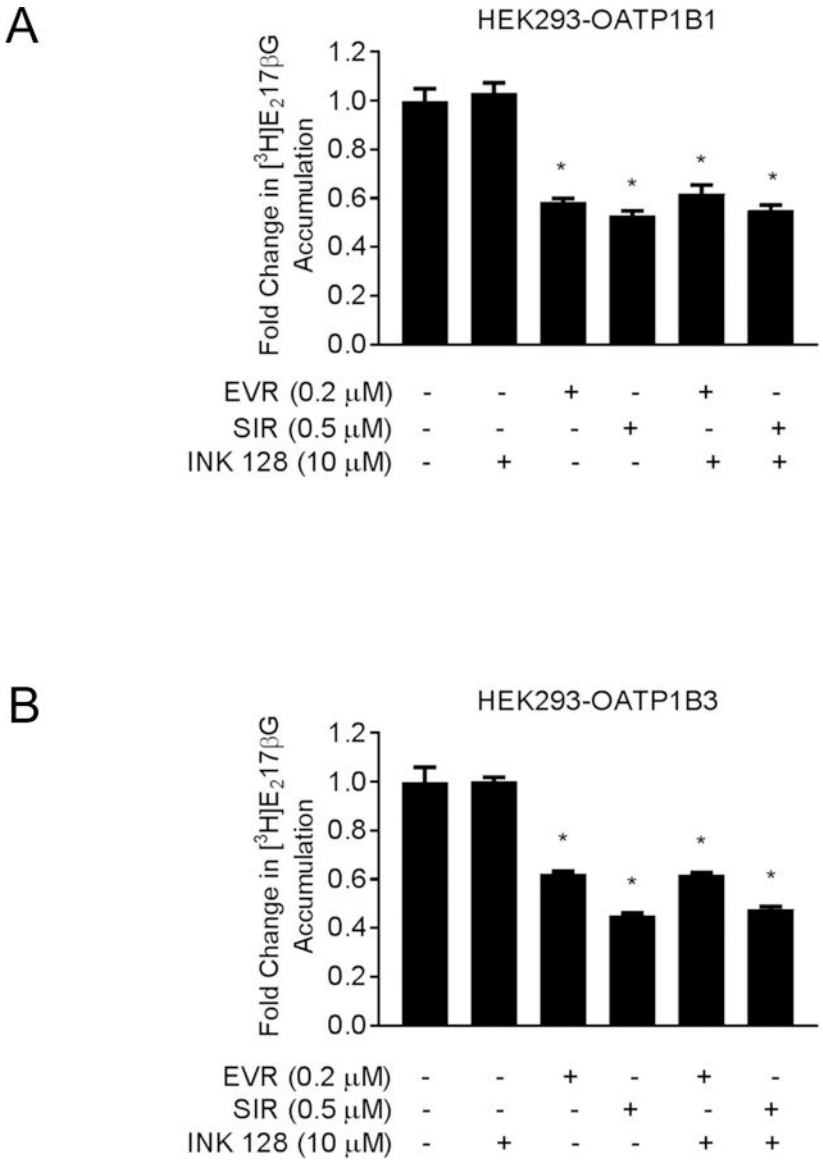


**Fig. 7. Effects of dual mTOR inhibitor INK-128 on pre-incubation effects of EVR and SIR.**

Model-estimated fold change and associated *SE* of the accumulation of [$^3$H]-$E_2$17βG (1 μM, 2 min) (A) and [$^3$H]-CCK-8 (1 μM, 3 min) (B) in HEK293-OATP1B1 and HEK293-OATP1B3 cells, respectively. The cells were pre-incubated with vehicle CTL-, 0.2 μM EVR-, or 0.5 μM SIR-containing culture medium for 1 hour either alone or in combination with 10 μM INK-128, following an earlier 1-hour treatment with 10 μM INK-128 alone. At the end of pre-incubation, the culture medium was removed and substrate accumulation was determined ($n$=3 in triplicate) in the absence of inhibitors after washing. Fold changes and SE were estimated using a generalized linear mixed model, as described in the "Materials and Methods". * indicates a statistically significant difference ($p$<0.05) vs. CTL.

**Table 1.**

EVR and SIR $IC_{50}$ values against OATP1B1-mediated transport of [$^3$H]-$E_2$17βG, [$^3$H]$E_1$S, [$^3$H]-rosuvastatin and OATP1B3-mediated transport of [$^3$H]-CCK-8 in HEK293-OATP1B1 and HEK293-OATP1B3 cells, respectively. $IC_{50}$ values are expressed as the mean ± SE from the model estimation (n=3 in triplicate). Determination of co- and pre+co- $IC_{50}$ values and Rvalues were calculated as described in the Materials and Methods. * indicates a statistically significant difference (p<0.05 by t-test) vs. coincubation values.

| | | Co-Incubation | | Pre+Co-Incubation | |
|---|---|---|---|---|---|
| **Transporter/Substrates** | | **$IC_{50}$ (μM)** | **R** | **$IC_{50}$ (μM)** | **R** |
| Everolimus | | | | | |
| OATP1B1 | $E_2$17G | 0.48 ± 0.07 | 1.09 (1.06−**1.15**) | 0.23 ± 0.06* | **1.19 (1.16–1.26)** |
| OATP1B1 | $E_1$S | 0.61 ± 0.08 | 1.07 (1.04−**1.17**) | 0.16 ± 0.02* | **1.27 (1.18–1.52)** |
| OATP1B1 | Rosuvastatin | 1.58 ± 0.92 | 1.03 (1.02–1.09) | 0.19 ± 0.07* | **1.23 (1.10–1.42)** |
| OATP1B3 | CCK-8 | 0.51 ± 0.08 | 1.09 (1.07−**1.11**) | 0.19 ± 0.02* | **1.23 (1.21–1.25)** |
| OATP1B1[a] | $E_1$S | 4.1 ± 1.1[a] | 1.01 | ND | ND |
| OATP1B3[a] | MPA | 3.7 ± 1.3[a] | 1.01 | ND | ND |
| Sirolimus | | | | | |
| OATP1B1 | E217G | 0.64 ± 0.16 | 1.00 (1.00–1.01) | 0.22 ± 0.04 | 1.01 (1.01–1.02) |
| OATP1B1 | $E_1$S | 0.83 ± 0.10 | 1.00 (1.00–1.01) | 0.65 ± 0.12 | 1.00 (1.00–1.01) |
| OATP1B1 | Rosuvastatin | 0.56 ± 0.30 | 1.00 (1.00–1.03) | 0.32 ± 0.11 | 1.01 (1.01–1.03) |
| OATP1B3 | CCK-8 | 0.97 ± 0.20 | 1.00 (1.00–1.01) | 0.36 ± 0.05* | 1.01 (1.00–1.01) |
| OATP1B1[a] | $E_1$S | 9.8 ± 1.1[a] | 1.00 | ND | ND |
| OATP1B3[a] | MPA | 1.3 ± 1.2[a] | 1.00 | ND | ND |

[a], data from a previous publication[24]; MPA, mycophenolic acid 7-o-glucuronide

**Table 2.**

Parameters values used for the EVR PBPK simulations

| EVR | Values | Reference/Comments |
|---|---|---|
| Dose (mg) | 10 | Ref.[16] |
| Chemical Structure | | 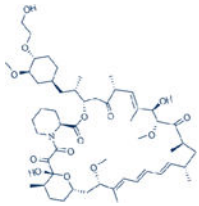 |
| **Physicochemical properties** | | |
| MW (g/mol) | 958.22 | Ref.[81] |
| Log $P_{O:W}$ | 4.23 | Calculated using ACD software[40] |
| Compound type | Neutral | Ref.[82] |
| Blood-to-plasma ratio ($C_b/C_p$) | 3.4 at 5 ng/ml | Ref.[38], see text for details |
| | 4.55 at 50 ng/ml | |
| | 4.58 at 100 ng/ml | |
| | 1.9 at 500 ng/ml | |
| | 1.1 at 1 μg/ml | |
| | 0.71 at 5 μg/ml | |
| Hematocrit value (%) | 45 | Simcyp default value |
| $f_u$ | 0.26 | Ref.[42] |
| **Absorption [Advanced dissolution, absorption and metabolism (ADAM) model]** | | |
| $f_{u,gut}$ | 1 | Assumed value |
| $P_{eff,man}$ ($x10^{-4}$ cm/s) | 6.67 | Predicted using the Simcyp mechanistic $P_{eff}$ (MechPeff) model Jejunum 1 regional permeability using logP input |
| **Distribution (minimal PBPK with single adjusting compartment)** | | |
| $V_{ss}$ (L/kg) | 1.55 (CV 36.0%) | Ref.[83] |
| $V_{sac}$ (L/kg) | 1.529 | Optimised in Simcyp Simulator |
| $k_{in}$ (1/h) | 0.493 | Optimised Ref.[41] |
| $k_{out}$ (1/h) | 0.0993 | Optimised Ref.[41] |
| $K_{p,liver}$ | 1 | Default value |
| **Elimination** | | |
| CL/F (L/h) | 15.4 (CV 34.3%) | Ref.[38] |
| $CL_R$ (L/h) | 0 | Ref.[45] |
| **Transport** | | |
| Intestinal efflux intrinsic clearance | | |
| $CL_{int,T,P\text{-}gp}$ (μL/min) | 7 | Optimised for 10 mg daily dose at steady state[47] and 10 mg weekly dose[38], verified against 10 mg steady-state dose in an independent study Ref.[49] |
| **Interaction** | | |
| $K_{i,OATP1B1}$ (μM) | 0.022 | Calibrated by CsA |

| EVR | Values | Reference/Comments |
|---|---|---|
| $K_{i,OATP1B3}$ (μM) | 0.044 | Calibrated by CsA |
| CYP3A4 | | |
| $K_i$ (μM) | 0.09 | Ref.[47] |
| $f_{u,mic}$ | 0.14 | |
| CYP3A5 | | |
| $K_i$ (μM) | 0.09 | Ref.[47] |
| $f_{u,mic}$ | 0.14 | |

$P_{O:W}$: neutral species octanol:buffer partition coefficient

$f_{u,gut}$: unbound fraction of drug in enterocytes

$P_{eff,man}$: human jejunum effective permeability

$V_{ss}$: volume of distribution at steady state

$V_{sac}$: volume of distribution of single adjusting compartment

$K_{p,liver}$: liver-plasma concentration ratio

**Table 3.**

Effects of preincubation with EVR and SIR on transport kinetics of OATP1B1 and OATP1B3. $K_m$ and $V_{max}$ values of OATP1B1-mediated $E_2$17ßG transport and OATP1B3- mediated CCK-8 transport in vehicle control (CTL), EVR (1 μM, 1 h) and SIR (1 μM, 1 h) preincubated HEK293-OATP1B1 and -OATP1B3 cells are shown. Experiments were conducted in triplicate. Data represent mean ± SD from 3 and 5 independent experiments for OATP1B1 and OATP1B3, respectively. *, p<0.05 by one-way ANOVA followed by Dunnett's test vs. CTL.

| Transporter | $K_m$ (μM) | | | $V_{max}$ (pmol/mg P/min) | | |
|---|---|---|---|---|---|---|
| | CTL | EVR | SIR | CTL | EVR | SIR |
| OATP1B1 | 3.3 ± 1.3 | 9.7 ± 1.8* | 9.2 ± 4.3* | 46.9 ± 11.8 | 32.3 ± 9.0* | 31.9 ± 5.1* |
| OATP1B3 | 5.8 ± 2.1 | 24.2 ± 8.7* | 22.9± 8.5* | 49.8 ± 16.6 | 39.9 ± 3.8 | 50.5 ± 5.3 |

**Table 4.**

Site of phosphorylation identified in OATP1B1 by LC-MS/MS. Mascot score, phosphoRS probability, ion mass and peptide mass accuracy were shown for representative phosphopeptides. Results from two independent experiments (n=2) are shown.

| Phosphorylation Site | Mascot Score[a] | PhosphoRS Probability[b] | Ion Mass (Da) | Peptide Mass Accuracy (ppm)[c] |
|---|---|---|---|---|
| S293 | 147.53 | 99.95% | 2933.4184 | 1.8 |
| S295 | 62.56 | 99.99% | 3013.3798 | 0.1 |
| T301 | 29.22 | 99.33% | 2933.4131 | 1.5 |
| T439 | 81.98 | 33.33% | 2114.9113 | 1.0 |
| T441 | 81.98 | 33.33% | 2114.9113 | 1.0 |
| Y442 | 81.98 | 33.33% | 2114.9113 | 1.0 |
| Y590 | 36.59 | 99.99% | 2229.1441 | −3.5 |
| S659 | 105.34 | 100.00% | 2424.9364 | −1.2 |
| S663 | 105.34 | 100.00% | 2424.9364 | −1.2 |

[a]The Mascot score is expressed as $-10*LOG_{10}(P)$, where P is the absolute probability that the observed match is a random event. Mascot scores greater than 67 are significant ($p<0.05$), suggesting that the null hypothesis that observed match is a random event had a probability of less than 5%[84].

[b]phosphoRS probability

[c]Peptide mass accuracy= $10^6$

[*]$(M_i-M_a)/M_a$ in ppm, where $M_i$ and $M_a$ are the observed and calculated mass, respectively, in Da[85]. The absolute mass accuracy value of less than 4 indicates accurate peptide assignments